J. Fluid Mech. (1974), *vol.* 63, *part* 1, *pp.* 51–79
Printed in Great Britain

Ice stalactites: comparison of a laminar flow theory with experiment

By SEELYE MARTIN
Department of Oceanography, University of Washington, Seattle

(Received 10 April 1973 and in revised form 8 August 1973)

Recent field observations in the polar oceans show that the hollow tubes of ice called ice stalactites form around streamers of cold brine rejected by the growing sea ice. In a laboratory study of this process, we inject cold, dense brine at a constant salinity, temperature and volume flux into an insulated tank of sea water held at its freezing point, then photograph the resultant stalactite growth. Because the inner wall temperature of the stalactite remains on the salinity-determined freezing curve, as the stalactite grows and the temperature deficit of the brine goes into the growth of ice, the inner wall melts to dilute and cool the adjacent brine back to its freezing point. This melting means that both the inner and outer stalactite radii increase with time. The radius of the stalactite tip, which is constant for each experiment, is shown to be controlled by the onset of a convective instability. If the tip becomes too large, overturning occurs and the sea-water intrusion freezes, reducing the radius of the tip so that the flow leaving the tip is marginally stable. Inside the stalactite, since the inner radius increases with time, both theory and experiment show the interior flow to be convectively unstable. The present study also derives a solution from the constant-heat-flux Graetz solution for the growth in both length and side-wall area of the stalactite. The experiments show that away from the stalactite base and the very beginning of the experiment this solution, with convection accounted for by an adjustable coefficient, describes the experimental growth. Finally, analysis of the experiments shows that as much as 50 % of the ice represented by the cold brine does not go into the stalactite, rather the ice goes directly into the ocean as loose crystals.

1. Introduction

During the past 15 years, scuba divers working under the pack ice of both the Arctic and Antarctic Oceans have reported the existence of long hollow tubes of ice growing from the bottom of the pack. Paige (1970), who calls these tubes 'stalactites', observed stalactites 10–100 cm in length in McMurdo Sound, Antarctica. Dayton & Martin (1971) give both photographs and descriptions of much larger stalactites in McMurdo Sound ranging from 1·5 to 6 m in length. Both papers report that the ice stalactites form and grow around streams of very cold brine draining from the pack.

In the following sections, we compare the results of a laboratory study of ice

stalactites with a theoretical model. First, § 2 describes the physics of how the stalactites form and grow. To grow stalactites, we injected cold brine at a constant flow rate into a tank filled with sea water at its freezing point. As § 3 describes, the brine was dyed and the stalactite lit in such a way that both the inner and outer stalactite walls are visible in the photographs. Figures 5, 6, 11, 13, 14 and 16 (plates 1–6) show sequences of photographs of the growth of the laboratory stalactites under various conditions.

Our theoretical model divides into two parts: first, a study of the growth of the tip, and second, a model of the overall growth of the stalactite. Examination of the sequences of photographs shows that although the inner radius of a particular stalactite at any depth increases with time, the radius of the tip remains nearly constant. Following our discussion in § 4 of the material properties of the ice and brine related to the stalactite growth, in § 5, we derive a criterion for the tip radius based on our observation that the tip radius adjusts itself so that the brine leaving the tip is marginally stable to overturning. We also show that the increase with time of the inner radius of the stalactite means that the interior flow is convectively unstable.

In § 6, we derive a model of the stalactite growth based on the constant-flux Graetz solution (Kays 1966; Goldstein 1938). In § 6.1 we derive the boundary conditions on the brine generated by the ice walls; and in § 6.2, a solution describing the growth in both the stalactite length and side-wall area.

In § 7, we compare our experimental results with the theoretical models. Section 7.1 shows that the observed and predicted tip radii are in good agreement, while § 7.2 shows that the interior flow is convectively unstable. In § 7.3, we show that the stalactite solution derived from the Graetz theory, with an adjustable coefficient which is constant for the different experimental runs, describes the stalactite growth away from both the very beginning of the experiment and the stalactite base.

2. How stalactites grow

When sea ice grows, as Weeks (1968) describes in a review article, salt is not directly incorporated into the ice; rather some of the sea water is trapped in small pockets of brine contained in a fresh ice crystal structure. For the trapped brine to remain in thermodynamic equilibrium with the ice, the salinity must increase by roughly 10‰ per °C depression of the temperature. This thermodynamic boundary condition is often called the 'Nernst' condition (see Frank (1950) for discussion and references); the curve on which temperature and salinity are in equilibrium, the eutectic curve.

As the sea ice increases in thickness through the polar winter, the trapped brine becomes colder and thereby more concentrated. Through processes which are not well understood, some of this brine escapes to the underlying ocean through systems of tubes called 'brine channels'. Lake & Lewis (1970) show photographs of these channels from field observations; Eide & Martin (1974) show photographs from a laboratory study.

Under winter sea ice, the sea-water temperature is at its freezing point. If the

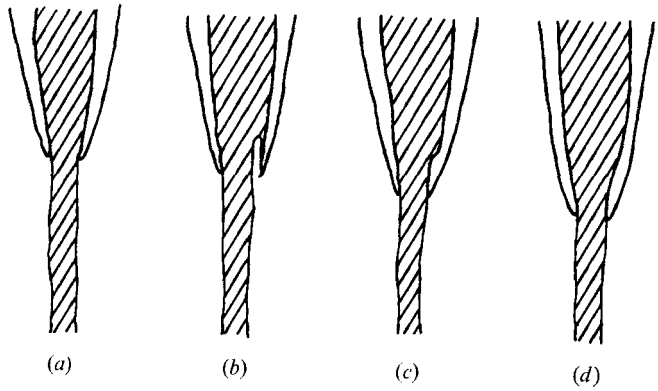

FIGURE 1. The sequence of sketches shows how the onset of overturning followed by the freezing of the sea-water intrusion controls the inner radius of the tip.

brine entering the sea water is colder than the sea water, the brine streamer gains heat only by freezing ice around itself, so that, as brine flows into the ocean, a stalactite forms and increases in both length and volume. As the stalactite photographs show, the inner radius of the stalactite at any depth also increases with time. The reason for this increase is as follows: since the walls of an ice tube transmit heat but not salt, immediately after a tube forms, relatively warm brine is in contact with the inner ice wall. To cool and dilute this brine back to the eutectic curve, the inner wall melts, with the heat of melting coming from ice accretion at the outer wall. Therefore, the salinity and temperature differences across the stalactite wall cause ablation of the inner wall and accretion at the outer wall.

At any depth, the stalactite walls begin their radial growth from the formation of the tip. From our observations, the tip grows asymmetrically; as brine flows from the stalactite, delicate crystals first grow as far as 1 cm down one side of the stream, and then ice fills in the gaps between the crystals until a tube extends completely around the stream. Therefore, the stalactite increases in length in spurts, first extending crystals from a tubular base, and then filling in the gaps. Because of this asymmetric growth, small fluctuations occur in the radius of the tip. The stalactite photographs show in spite of these fluctuations that the inner radius of the tip remains nearly constant in the course of a particular experiment.

Our observations suggest that the onset of a convective instability determines the size of the tip. We observe for a constant volume flux, if the radius of the tip is small enough, that the flow emerges as a uniform stream. On the other hand, if the radius fluctuates above a certain critical value, then overturning occurs and sea water intrudes up into the tip. Figure 1, an idealized schematic drawing of the tip, shows how the onset of the overturning controls the tip radius. Because the sea water is both warmer than the brine and at its freezing point, when a sea-water intrusion occurs, it freezes, and thereby reduces the radius of the tip back to the size at which overturning does not occur.

At the same time as convective overturning acts to maintain the tip radius below a certain value, two processes keep the tip radius as large as possible.

First, the salinity-driven ablation of the inner wall constantly increases the radius. Second, if we assume Poiseuille flow in the tip, then for a constant volume flux, the shear stress on the delicate ice crystals which make up the walls of the tip goes as a^{-4}, where a is the inner radius. Therefore, the larger the radius, the lower the stress on the crystals, and the less likelihood of the crystals breaking off.

The combination of the convective instability and both the shear stress and the salinity-driven ablation means that the tip radius responds very rapidly to changes in the volume flux rate. We found if we increased the flow rate during an experimental run that within seconds the tip radius grew to a larger equilibrium radius. The tip responds with similar speed to a decrease in flow rate. As an example, the last photograph in figure 14 (plate 5) shows the extreme case where we turned off the pump. At this point, massive overturning occurred and with the exception of a very small drainage channel, the lower 2–3 cm of the stalactite were blocked off.

Once the walls form, our observations suggest that they grow through conductive heat transfer. As figure 14 shows most clearly, needle-like, nearly radially oriented ice crystals make up the stalactite wall. The presence of these needles suggests that the wall growth results from radially symmetric heat conduction. Finally, a large fraction of the heat transferred to the cold brine does not go into stalactite growth, but rather goes into the formation of ice crystals both at the tip and inside the stalactite. These crystals, which are swept into the interior of the tank, where they then rise slowly to the surface, form the ice clouds shown in the stalactite photographs.

3. The experiments

As figure 2 shows, our experiments took place in a large polyurethane-insulated tank. A sodium chloride solution with a salinity of 34·8 ‰ and a freezing point of $-1{\cdot}9\,^{\circ}\mathrm{C}$ filled the tank. This solution, which we shall hereafter call 'sea water', has the salinity and freezing temperature of the water in McMurdo Sound. On top of the sea water, we anchored a polyurethane lid, through which we injected cold brine thus growing stalactites. An overflow valve kept the sea water in the tank at a constant height.

We placed the entire apparatus in a cold room, and set the cold room temperature, which was steady to within $0{\cdot}5\,^{\circ}\mathrm{C}$, at the desired brine temperature. A constant-volume-flow peristaltic pump transported the brine through an uninsulated tube from an open beaker to the tank. Inside the tank, the sea-water temperature, as both a thermometer and the presence of small ice crystals in and on the sea water showed, stayed within $0{\cdot}1\,^{\circ}\mathrm{C}$ of its freezing point. Therefore, the cold brine could only gain heat by freezing ice from the surrounding sea water.

The stalactite grew from the bottom of a polyurethane block which extended 3 cm below the bottom of the lid. Preliminary observations showed that at the flow rates used in the experiment the brine inside the stalactite is nearly in hydrostatic equilibrium with the sea water outside. The polyurethane block increased the sea-water pressure head and thus prevented the brine level inside

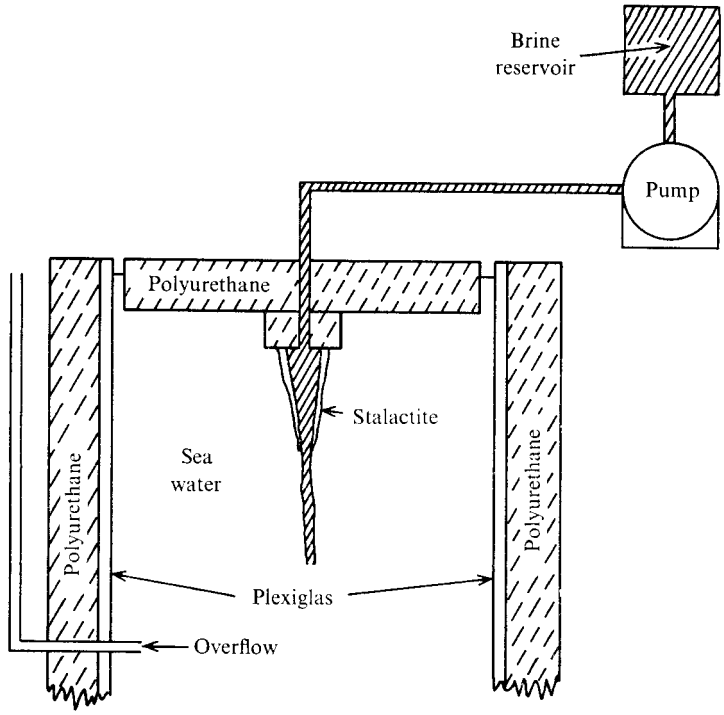

FIGURE 2. A schematic diagram of the experimental apparatus.

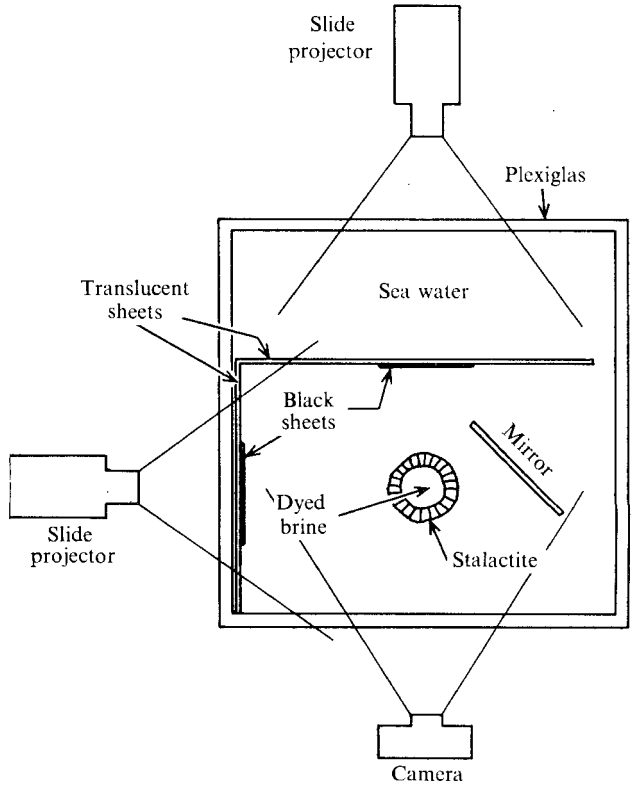

FIGURE 3. A schematic diagram of the photographic lighting arrangement.

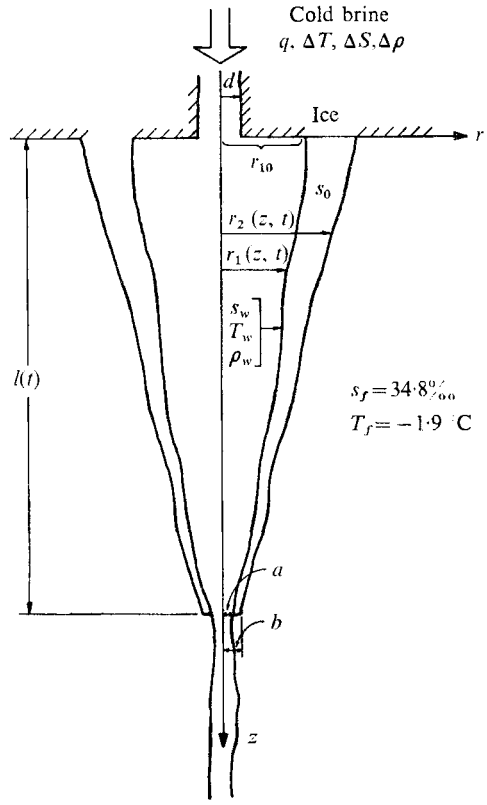

FIGURE 4. A schematic diagram of a typical stalactite.

the stalactite-feeder tube system from dropping below the base of the stalactite. On the bottom of this block, we cut a notch running from the input tube to the outer edge of the block. When the pump is first started, this notch permits the escape of any air bubbles trapped in the feeder tube.

The feeder tube which extended through the block was glass, with an inner radius of $1{\cdot}5 \times 10^{-1}$ cm. This value is consistent with Partch's (1972, private communication) observations made in the Beaufort Sea. The stalactites he observed resembled those shown in the last frames of figures 6 and 13 (plates 2 and 4), with inner diameters of the order of centimetres. When he broke off these stalactites, he found, however, that the inner diameter of the brine channel inside the ice was only of the order of millimetres.

Before beginning an experiment, to provide an initial nucleation surface, we froze a layer of fresh water onto the block. Also, in some experiments, the polyurethane block on which the stalactite grew was removable, so that, after growing a stalactite, we could recover the stalactite, melt it and then measure both its bulk salinity and total weight. From these measurements, which the fragility of the stalactite made difficult, we determined what fraction of the heat transferred to the brine went into stalactite growth as opposed to the fraction rejected as free ice crystals.

As §§ 6 and 7 show, measurements of both the inner and outer radii at different depths and the length of the stalactite allow us to compare the observed stalactite growth with theory. We made these measurements from photographs taken in the following way. For contrast, following Baker (1966), we dyed the brine with thymol blue and made the sea water slightly acidic, so that the brine was dark blue and the sea water was light yellow. When we back-lighted the stalactite with a diffuse light, the radially oriented crystals of the stalactite wall at right angles to the light glowed, while the other crystals transmitted light, thus defining the inner wall profile. To define the outer wall, we photographed the stalactite against a dark background. Figure 3 shows the combination of these two processes: our lighting consisted of a diffuser screen with a narrow black strip running down the middle, lit from behind with a slide projector. To check for radial symmetry, we placed a mirror in the tank, and set up a duplicate lighting system at right angles to the first, so that our photographs provided two views of the stalactite. To provide a time and length scale in our photographs, we also placed a stop watch and a ruler inside the tank next to the stalactite.

At the beginning of a typical experiment, we started the pump and the watch simultaneously. Quite often, air bubbles or small pieces of ice would be rejected from the feeder tube, so that the first few seconds of the stalactite growth were chaotic. Generally, after this initial disturbance, a cylindrical tube of ice would begin to grow around the brine stream. Depending on the rate of growth, we took photographs at intervals ranging from 10 s to 3 min. We terminated the experiment when the stalactite grew to a length of 15–18 cm. At the end of the experiment, the pump was calibrated.

4. Properties of the ice and brine

Figure 4 is a schematic diagram of a stalactite. Brine flows into the stalactite at a volume flux rate q and a temperature and salinity difference relative to the sea water of ΔT and Δs. $\Delta\rho$ is the density difference between the brine and the sea water and $\Delta\rho_w$ is the density difference between the brine and the fluid at the inner wall. Outside the stalactite, the sea water is at its salinity-determined freezing point of T_f and s_f. The ice walls have a bulk salinity s_0, and at the inner wall, the temperature and salinity are T_w and s_w. We assume that the stalactite is axially symmetric, with z and r as the axial and radial variables. The inner and outer radii of the stalactite are r_1 and r_2, respectively; the inner and outer radii of the tip are a and b. The length of the stalactite is $l(t)$. The inner radius of the tube through which the brine flows into the sea water is d, and that of the stalactite directly under the ice is r_{10}.

In our experiments, the temperatures and salinities of the brine solutions range from $-20\,^\circ$C and 224‰ to $-2\,^\circ$C and 35‰. For this range, the following brine properties have nearly constant values. Kaufman (1960, p. 608) gives the specific heat $c_p = 0{\cdot}9\,\mathrm{cal\,g^{-1}\,^\circ C^{-1}}$, the thermal conductivity

$$k = 1{\cdot}3 \times 10^{-3}\,\mathrm{cal\,cm^{-1}\,s^{-1}\,^\circ C^{-1}},$$

Salinity (‰)	Freezing temperature (−°C)	$\Delta\rho$ at freezing (g cm^{-3} × 10^{-2})	ν (cm^2 s^{-1} × 10^{-2})	
			At freezing	At −2°C
224	20	15	6·8	3·2
188	15	12	4·6	2·7
140	10	8	3·2	2·3
79	5	3	2·3	2·1
35	2	—	1·8	1·8

TABLE 1. Freezing temperature, density difference and viscosity as a function of salinity (from Kaufman 1960, p. 608). The density at −2 °C and 35‰ is $\rho = 1{\cdot}03$ g cm^{-3}

the thermal diffusivity $\kappa = 1{\cdot}3 \times 10^{-3}\,\mathrm{cm^2\,s^{-1}}$ and the salt diffusivity

$$D \simeq 10^{-5}\,\mathrm{cm^2\,s^{-1}}.$$

The freezing temperature, density difference and viscosity of brine vary greatly over this range; table 1 lists their values as a function of salinity.

The material properties of the ice, such as the latent heat L, the conductivity k_i, the specific heat c_{pi} and the thermal diffusivity κ_i, strongly depend on both the mean ice temperature and the bulk salinity of the ice s_0. Weeks (1968) describes the physical process by which salt is trapped within the ice, and Weeks & Lofgren (1967) measure s_0 as a function of the growth velocity v for one-dimensional ice growth. Their results show when $v = 8 \times 10^{-4}\,\mathrm{cm\,s^{-1}}$ that the entrained salinity $s_0 = 0{\cdot}95 s_f$. On the assumption that their measurements made with an ice front advancing downward are applicable to our stalactites, where the ice advances radially outward with $\partial r_2/\partial t$ ranging from $0{\cdot}5 \times 10^{-3}$ to $5 \times 10^{-3}\,\mathrm{cm\,s^{-1}}$, then for the stalactites, s_0 should be of the order of s_f.

Two laboratory stalactites grown from −20 °C brine, where $\partial r_2/\partial t \sim 10^{-3}\,\mathrm{cm\,s^{-1}}$, were recovered, melted and the average s_0 measured. Using the removable core described in the previous section, when the pump was stopped, we gently removed the stalactite into the −20 °C air of the cold room and suspended it until it became solid ice. This had two effects: first, sea water coated and froze onto the stalactite surface; second, some brine appeared to drip from the stalactite. The sea water adhering to the outside would increase the stalactite salinity; while the brine expelled by the cooling of the stalactite would decrease the average salinity. For both of our experimental recoveries, we measured $s_0 = 27$–28‰, which is of the expected order. In what follows, we assume that the bulk salinity of the ice is 28‰.

To calculate L, k_i, c_{pi} and κ_i for $s_0 = 28$‰ and the experimental range of temperature, we use the following sources. First, Ono (1967) discusses the change of phase of sodium chloride solutions. Because solutions change phase over a range of temperatures, Ono redefines the term 'latent heat' as "the heat necessary to melt one gram of ice of a given bulk salinity and temperature". Using this definition, he gives an empirical relation for L as a function of salinity and temperature in the range $0 \geqslant T \geqslant -8$ °C. He also gives a similar relation for c_{pi} in the same range.

T ($-$ °C)	s (‰)	L (cal g^{-1})	c_{pi} (cal g^{-1} °C^{-1})	k_i (cal cm^{-1} s^{-1} °C^{-1} $\times 10^{-3}$)	L/k_i (cm °C s g^{-1} $\times 10^4$)	κ_i (cm^2 s^{-1} $\times 10^{-3}$)
2	28	17·4	30	1·98	0·88	0·01
4	28	50·6	8	3·18	1·59	0·4
6	28	61·7	3·8	3·58	1·73	1·1
8	28	67·8	2·4	3·77	1·80	1·6
0	0	80·0	0·5	4·36	1·83	9·5

TABLE 2. Material properties of sea ice at selected temperatures and salinities

Second, on the assumption that parallel columns of ice separated by tubes of brine make up the ice, Schwerdtfeger (1963) calculates the thermal conductivity of salt ice in terms of the fresh-ice value $k_f = 4{\cdot}2 \times 10^{-3}$ cal cm^{-1} s^{-1} °C^{-1} and k.

Third, the definition of the thermal diffusivity is

$$\kappa_i \equiv k_i/\rho_i c_{pi},$$

where Schwerdtfeger also shows that the density ρ_i of salt ice varies by only a few per cent from the fresh-ice value 0·917 g cm^{-3}.

Table 2 lists L, k_i, c_{pi} and κ_i at several temperatures and at two salinities. We also give the product L/k_i, which occurs in our theory and as the table shows, varies by much less than L. From both table 2 and the above equations, we see that, as the temperature of the sea ice approaches the temperature of sea water, L goes to zero and $k_i = k$. As the salt ice becomes very cold, L tends to the fresh-ice value plus a specific heat term, which is small for our range of salinities and temperatures, and k_i tends to the fresh-ice value. Finally, the values of κ_i vary greatly over the range of interest.

5. Convection in the stalactite

As § 2 describes, the onset of overturning and the intrusion of sea water into the stalactite at the tip keep the inner radius nearly constant. Also, the combination of the Nernst condition and the heat flux through the walls inside the stalactite means that the fluid adjoining the inner wall is warmer, less saline and therefore more buoyant than the interior brine, so that as the diameter of the stalactite increases, overturning also occurs in the interior.

To derive a criterion for the onset of overturning, we assume that the unperturbed flow in the stalactite is Poiseuille flow with a uniform pressure-gradient force per unit volume

$$\frac{\partial p}{\partial z} = \frac{8}{\pi}\frac{\rho \nu q}{r_1^4}.$$

In the stalactite, we assume that this force acts on a fluid element at the inner wall. At the tip, the density difference between the brine and the sea water generates an opposing buoyancy force $\Delta\rho g$ per unit volume and at an ablating

inner wall, melting generates a similar force $\Delta\rho_w g$. The ratio of the buoyancy to the pressure-gradient force gives the following dimensionless parameter:

$$E = \tfrac{1}{8}\pi\Delta\rho_w g r_1^4/\rho\nu q, \tag{1}$$

where, following Ellison & Turner (1959), we call E an entrainment number. At the tip, $r_1 = a$ and $\Delta\rho_w = \Delta\rho$. When $E > 1$, we assume that overturning occurs; when $E < 1$, the downward flow entrains the less dense fluid and the flow is a modified Poiseuille flow. Because the fluid at the inner wall is warmer, less saline and thereby from table 1 generally much less viscous than the interior flow, the Poiseuille profile only approximates the interior flow.

The related problem of the stability of the flow of water down a vertical pipe with constant side-wall heating, where both the temperature and velocity profiles are fully developed, has been extensively studied. The work of Hallman (1958) and Scheele & Hanratty (1963), who studied this problem experimentally, and Scheele, Rosen & Hanratty (1960), who reviewed the theoretical research, shows for this case that instabilities develop at a constant value of E. In our problem, the low salt diffusivity restricts buoyancy effects to a wall boundary layer, so that the above results cannot be used directly to predict the onset of instability.

Application of (1) to the stalactite involves three additional assumptions. First, we neglect salt diffusion in the overturning by the following argument. The Reynolds number inside the stalactite is

$$R_e = 2q/\pi r_1 \nu,$$

where for the experiments $q \sim 0{\cdot}1$–$1\,\mathrm{cm^3\,s^{-1}}$, $r_1 \simeq 0{\cdot}5\,\mathrm{cm}$ and the viscosity follows from table 1, so that $R_e \sim 10$–10^2. Because $R_e > 1$ and $D/\nu \sim 10^{-3}$ diffusion will be negligible compared with viscosity and the balance (1) will dominate the overturning. Only for very slow flows, or $R_e \ll 1$, would we expect diffusion to be important.

Second, we assume that during a stalactite experiment the volume flux Δq generated by the inner wall ablation is much less than q. When an element of ice melts at the inner wall, its volume decreases by roughly 10%. This change in volume means that slightly less fluid leaves at the tip than enters the stalactite. If we consider a stalactite of length 10 cm, average radius 0·5 cm and with an average inner wall velocity of $10^{-4}\,\mathrm{cm\,s^{-1}}$, then $\Delta q \sim 10^{-4}\,\mathrm{cm^3\,s^{-1}}$. Since $q \sim 10^{-1}\,\mathrm{cm^3\,s^{-1}}$, Δq is only 0·1% of q, so that q is nearly constant throughout an experiment.

Third, we assume that the inner wall ablation has a negligible effect on $\Delta\rho$ measured at the tip. On the worst-case assumption that the walls are pure ice, then using the same scales as the preceding paragraph, the volume flux of fresh water into the stalactite from side-wall melting is of order $10^{-3}\,\mathrm{cm^3\,s^{-1}}$, which is only 1% of q. Therefore, the mean density difference should also be nearly constant when measured at the tip.

If we assume that the fluid leaving the tip is marginally stable according to (1), then we may easily show that the interior flow is unstable. Because of the inner wall ablation, the inner radius constantly increases with time. The fourth-power

dependence of r_1 in (1) means that, if r_1 doubles from its value at the tip, then for the flow to remain stable, $\Delta\rho_w$ must decrease to $\frac{1}{16}\Delta\rho$. In the experiments, however, we observe that $\Delta\rho_w \gtrsim \frac{1}{2}\Delta\rho$. Therefore, the interior flow must be unstable. In spite of this convective instability, we find in the following sections that a stalactite model based on the Graetz solution, which assumes a Poiseuille velocity profile, yields a good description of the stalactite growth.

6. The Graetz model

In the following two subsections, we first develop the boundary conditions on the brine flow imposed by the ice wall, then solve the governing equations for the stalactite growth.

6.1. *The boundary conditions*

At the ice wall, the boundary conditions divide into three groups: the previously discussed Nernst condition, which relates the temperature to the salinity at the ice–water interface, and the thermal and salinity boundary conditions, which we discuss below.

6.1.1. *The thermal boundary condition.* Inside the ice, the heat equation

$$\frac{\partial T_i}{\partial t} = \frac{\kappa_i}{r}\frac{\partial}{\partial r}\left(r\frac{\partial T}{\partial r}\right) + \kappa_i\frac{\partial^2 T_i}{\partial z^2}, \tag{2}$$

where t is time, describes the temperature field (Carslaw & Jaeger 1959, p. 17). If the heat flux through the wall is quasi-steady, then we can drop the left-hand side of (2). To calculate the relative magnitudes of the terms in (2), our observations show that the stalactites grown from $-20\,^\circ\mathrm{C}$ brines had a mean wall temperature of roughly $-8\,^\circ\mathrm{C}$ (see §7.2 for examples), which from table 2 corresponds to $\kappa_i = 10^{-2}\,\mathrm{cm^2\,s^{-1}}$. At a constant depth on the stalactite, we observed that

$$\Delta T/\Delta t = 5\times 10^{-2}\,^\circ\mathrm{C\,s^{-1}},$$

and over a $10^{-1}\,\mathrm{cm}$ change in r across the wall, T changed by $1\,^\circ\mathrm{C}$. Therefore,

$$\kappa_i\,\Delta T/(\Delta r)^2 \sim 1 \gg \Delta T/\Delta t, \tag{3}$$

so that the right-hand side of (2) is an order of magnitude greater than the left-hand side. For the stalactites grown from brines with smaller temperature differences, although table 2 shows that the value of κ decreases, our observations show that the stalactite growth decreases proportionally, so that the inequality (3) still holds.

Similarly, to eliminate the axial second derivative in (1), we note that typically ΔT changes by $1\,^\circ\mathrm{C}$ over a $1\,\mathrm{cm}$ change in z along the wall, and by the same amount over a $10^{-1}\,\mathrm{cm}$ radial change. Therefore,

$$\Delta T/(\Delta r)^2 \gg \Delta T/(\Delta z)^2.$$

The neglect of the time dependence and z dependence in (2) is invalid at both the tip and the very beginning of the experiment; however, over most of the stalactite, the heat equation (2) reduces to

$$\frac{\partial}{\partial r}\left(r\frac{\partial T_i}{\partial r}\right) = 0. \tag{4}$$

To derive the boundary conditions on (4), we neglect the internal freezing caused by cooling of the trapped brine in the ice wall and assume that ice only forms and melts at the outer and inner walls. At the outer wall, since the sea water is at its freezing point, all of the heat transferred through the ice comes from accretion, so that the boundary condition is

$$\frac{\partial T_i}{\partial r} = \frac{L\rho_i}{k_i}\frac{\partial r_2}{\partial t} \quad \text{at} \quad r = r_2. \tag{5}$$

At the inner wall, the heat flux from the outer wall is absorbed in two ways: partly by ablation of the inner wall and partly by warming of the interior brine. Formally, this boundary condition is

$$k_i\frac{\partial T_i}{\partial r} = L\rho_i\frac{\partial r_1}{\partial t} + k\frac{\partial T}{\partial r} \quad \text{at} \quad r = r_1, \tag{6}$$

where the non-subscripted temperatures and conductivities refer to the brine.

Substitution of the solution of (4) into (5) and (6) gives the following expression for the heat flux at the inner wall:

$$\frac{L\rho_i}{2k_i}\frac{1}{r_1}\frac{\partial}{\partial t}(r_2^2 - r_1^2) = \frac{k}{k_i}\frac{\partial T}{\partial r}\bigg|_{r=r_1}. \tag{7}$$

From (7), the heat flux to the brine is proportional to the rate of increase of the cross-sectional area of the stalactite. Also, because the salinity-driven ablation only transfers ice from the inner to the outer wall, (7) is an exact equation for the wall growth.

Similarly, we calculate the inner wall temperature as

$$T_f - T_w = \frac{L\rho_i}{2k_i}\log\left(\frac{r_2}{r_1}\right)\frac{\partial}{\partial t}r_2^2, \tag{8}$$

so that the inner wall temperature is independent of whether freezing or melting takes place at the inner wall.

As (7) and (8) show, measurements of r_1 and r_2 as functions of time determine both T_w and the heat flux to the interior brine.

6.1.2. *The salinity boundary condition.* Since the ice wall prevents conductive transfer of salt, the boundary condition on the salinity is much simpler than that on the temperature. A balance between the convective transfer of salt caused by the melting of the inner wall and the diffusive transport of salt away from the wall determines the salinity at the inner wall. Weeks & Lofgren (1967) and Kays (1966, p. 308) discuss this condition in greater detail and show for steady-state one-dimensional freezing or ablation that the boundary condition at the wall is

$$(s_w - s_0)\frac{\partial r_1}{\partial t} + D\frac{\partial s}{\partial r} = 0 \quad \text{at} \quad r = r_1. \tag{9}$$

6.2. *The stalactite solution*

In the general stalactite problem, the Nernst condition and the motion of the inner wall in (7) and (9) couple the equations of motion with the diffusion equations

for heat and salt. To simplify this complicated problem, we note that in many of our experiments the inner brine absorbs most of the heat generated by the growth of the outer wall. From (9), the ratio of the heat absorbed at the inner wall to that generated at the outer wall is

$$H = \frac{r_1 \partial r_1/\partial t}{r_2 \partial r_2/\partial t}. \tag{10}$$

In the experiments, $\partial r_1/\partial t \sim 10^{-4}\,\mathrm{cm\,s^{-1}}$, $\partial r_2/\partial t \sim 10^{-3}\,\mathrm{cm\,s^{-1}}$ and $r_1 \sim r_2$, so that $H \sim 10^{-1}$ in our experiments. Therefore, as a first approximation, we assume that all the heat generated by freezing goes to the brine. This assumption decouples the salinity from the temperature field, so that we can solve the thermal problem independently of the salinity.

In what follows, we apply the familiar Graetz solution (Kays 1966, p. 102; Goldstein 1938, p. 622) for Poiseuille pipe flow with constant side-wall heating; the Graetz solution gives a linear rise in mean fluid temperature with length down the tube. To apply this solution to the stalactite, we assume that the side-wall heat flux averaged around the stalactite at any depth is both independent of depth and causes the inner wall temperature of the brine to increase from its temperature at the entrance to the sea-water temperature at the tip.

The constant-heat-flux solution has physical appeal, since if the flux is greater at one depth than another, then the wall thickness increases more rapidly where the flux is greater, thus increasing the insulation and reducing the flux to some mean value. In our experiments, we observe even when $E > 1$ that the averaged side-wall flux is still approximately constant. Therefore, we might expect that some form of the model derived herein will describe the stalactite growth even when convection occurs.

For Poiseuille flow, following Goldstein (1938, p. 617), the temperature field is a solution of the heat equation

$$\frac{\partial T}{\partial t} + u\frac{\partial T}{\partial z} + v\frac{\partial T}{\partial r} = \kappa\left[\frac{\partial^2 T}{\partial r^2} + \frac{1}{r}\frac{\partial T}{\partial r} + \frac{\partial^2 T}{\partial z^2}\right], \tag{11}$$

where u and v are the axial and radial velocities.

From our observations, the rate of growth of the stalactite is much less than the mean brine velocity. This implies that the convected temperature terms are much greater than the time rate-of-change term, so that in the following analysis we drop the explicit time dependence in (11).

To simplify our subsequent analysis further, we both write our variables in non-dimensional form and carry out the following co-ordinate transformation:

$$z' = \frac{z}{(2/\pi)(q/\kappa)}, \quad u', v' = \frac{u, v}{(2/\pi)(q/r_1^2)}, \quad r' = \frac{r}{r_1(z,t)}, \quad \theta(r', z') = \frac{T_f - T}{\Delta T}, \tag{12}$$

where the primed terms are dimensionless. For future reference, the length scale $(2/\pi)(q/\kappa) = R_e P_r r_1$, where P_r is the Prandtl number ν/κ.

In the notation of (12), the axial flow profile is

$$u = 1 - r^2, \tag{13}$$

where, for convenience, we drop the primes from the dimensionless variables. The radial velocity v follows from the continuity equation and (13).

Substitution of these velocities into (11) gives

$$(1-r^2)\frac{\partial\theta}{\partial z} = \frac{1}{r}\frac{\partial}{\partial r}\left(r\frac{\partial\theta}{\partial r}\right) + O\left(\frac{1}{R_e^2 P_r^2}\right), \tag{14}$$

where the last term on the right represents the axial diffusion of temperature. Since $R_e \sim 10^2$ and $P_r \sim 10$, axial diffusion is negligible compared with radial diffusion. Equation (14), which describes low Reynolds number flow in our slightly convergent pipe, is identical with the Graetz equation for flow in a straight pipe.

To determine the rate of growth of the stalactite, we next apply boundary conditions at the entrance, side wall and exit of the stalactite. At the entrance, the brine enters the stalactite at a constant temperature and volume flux. Using heat transfer terminology, the fluid enters with a constant velocity-averaged or 'mixed-mean' temperature T_M, which we write in dimensional form as

$$T_M = \frac{2\pi}{q}\int_0^{r_1} u(T_f - T)\, r\, dr. \tag{15}$$

When measured at the stalactite tip, T_M is the temperature of a collected sample.

In terms of T_M, the boundary condition at the entrance is

$$T_M = q(\Delta T)\alpha \quad \text{at} \quad z = 0, \tag{16a}$$

where $\alpha \leqslant 1$.

The parameter α accounts for our observation that not all of the heat transferred to the cold entering brine goes into stalactite ice. Some heat is lost when sea water flows up into the interior, freezes and then is rejected as ice crystals. Still more heat is lost when stresses break off the fine crystals which make up the tip, and finally, some heat may be lost because the sea water is slightly above its freezing point. In the analysis, we assume that these processes extract heat from the brine at a constant rate so that, for any particular experiment, α is constant.

At the side wall, we assume that the heat flux averaged around the circumference of the tube at any z is a function of time only. In dimensionless variables, this condition becomes

$$\partial\theta/\partial r = -\tfrac{1}{4}B(t) \quad \text{at} \quad r = 1, \tag{16b}$$

where $B(t)$ is a function of time to be determined and the factor $\frac{1}{4}$ simplifies our subsequent work.

Finally, at the tip we apply two boundary conditions. First, we assume that the wall temperature of the brine equals the sea-water temperature, so that

$$\theta = 0 \quad \text{at} \quad z = l, \quad r = 1. \tag{16c}$$

Second we assume that the stalactite tip grows as a cylinder of constant cross-sectional area, with a growth rate proportional to the mixed-mean temperature measured at the tip. If $\pi(b^2 - a^2)$ is the cross-sectional area of the tip and ϵ is a constant of proportionality, then the following dimensional equation describes the growth of the tip:

$$\pi(b^2 - a^2)\,\partial l/\partial t = \epsilon F \theta_M(l), \tag{16d}$$

where θ_M is the dimensionless mixed-mean temperature and $F = \Delta T \rho c_p / L \rho_i$. The dimensionless constant F is the ratio of the flux of ice into the stalactite to the flux of fluid. For sodium chloride solutions, $F \leqslant 0{\cdot}3$. In our analysis, we also assume for a particular experiment that ϵ is constant.

The well-known solution of (14) which satisfies the boundary condition (16*b*) is

$$\theta = -Bz + g(r) + \theta_{w0}, \tag{17a}$$

where

$$g(r) = +B(\tfrac{3}{16} - \tfrac{1}{4}r^2 + \tfrac{1}{16}r^4), \tag{17b}$$

and $\theta_{w0}(t)$ is the to-be-determined entrance wall temperature. If we both write (15) in dimensionless form and substitute (17), then we find

$$\theta_M = \theta_{w0} - Bz + \tfrac{11}{96}B. \tag{18}$$

The number $\frac{11}{96}$ is an important constant. From Goldstein (1938, p. 623), the Nusselt number based on the mixed-mean temperature is

$$N_u = \tfrac{48}{11} = \tfrac{1}{2} \times \tfrac{96}{11}. \tag{19}$$

In the discussion of the experimental results, we show as a first approximation that replacement of the constant $\frac{11}{96}$ by $1/2N_u$, where N_u is a constant for a particular run, accounts for the increase in heat transfer caused by convection.

To simplify the analysis again, we both re-scale $l(t)$ and define a non-dimensional time τ as follows:

$$\lambda = l(t)/l_0, \quad \text{where} \quad l_0 = \tfrac{11}{48}q/\pi\kappa, \tag{20a}$$

and

$$\tau = t/\tau_0, \quad \text{where} \quad \tau_0 = \tfrac{11}{96}(b^2 - a^2)/\epsilon\alpha\kappa F, \tag{20b}$$

where $l(t)$ and t are dimensional quantities.

To solve for the functions B and θ_{w0}, we substitute (18) and (20) into the boundary conditions (16*a*, *c*) to obtain

$$B = \tfrac{96}{11}\alpha/(1+\lambda), \tag{21a}$$

$$\theta_{w0} = \lambda\alpha/(1+\lambda). \tag{21b}$$

From (18) and (21), the mixed-mean temperature at the tip is

$$\theta_M(l) = \alpha/(1+\lambda). \tag{22}$$

Substitution of (22) into (16*d*) gives the following expression for the stalactite length:

$$2\partial\lambda/\partial\tau = 1/(\lambda+1). \tag{23}$$

If $\lambda = 0$ at $\tau = 0$, then (23) has the solution

$$\lambda = (1+\tau)^{\frac{1}{2}} - 1. \tag{24}$$

In a dimensional form convenient for comparison with our data, (24) becomes

$$l^2/t = \beta^2 - 2l_0 l/t, \tag{25a}$$

where $\beta^2 = l_0^2/\tau_0$, and for $t \gg \tau$,

$$l^2/t = \beta^2. \tag{25b}$$

From both the preceding results and (7), we next calculate the variation in side-wall area with depth. If we define the non-dimensional side-wall area as

$$A = (r_2^2 - r_1^2)/(b^2 - a^2), \tag{26}$$

then substitution of (16b), (21a), (24) and (26) into the non-dimensional form of (7) gives

$$\frac{\partial A}{\partial \tau} = \frac{1}{2\epsilon(\lambda+1)} = \frac{1}{2\epsilon(1+\tau)^{\frac{1}{2}}}. \tag{27}$$

To integrate (27), we note that, when the stalactite tip reaches a depth z at some time τ^*, $A(\tau^*, z) = 1$. From (24), the lower limit of integration on (27) is therefore

$$A = 1 \quad \text{at} \quad \tau^* = z^2 + 2z. \tag{28}$$

Integration of (28) from τ^* to τ gives

$$A(\tau, z) = \epsilon^{-1}[(1+\tau)^{\frac{1}{2}} - (1+z)] + 1, \tag{29}$$

so that at a fixed depth the cross-sectional area has the same time dependence as the length. Differentiation of (29) with respect to z gives

$$[\partial A/\partial z]_\tau = -1/\epsilon, \tag{30}$$

so that the areal slope is a constant for a particular stalactite.

To explain the ϵ^{-1} term in (30), we note that the magnitude of ϵ affects only the growth of the tip, not the side-wall heat flux. Therefore, when $\epsilon \ll 1$, the stalactite grows very slowly in length relative to its increase in side-wall area, so that the walls become very wedge-like.

In dimensional terms, (30) becomes

$$\frac{\partial}{\partial z}(r_2^2 - r_1^2) = -\frac{b^2 - a^2}{l_0 \epsilon} = -\zeta, \tag{31}$$

where ζ, the dimensional areal slope, is constant for a particular experiment.

This completes the derivation of the stalactite solution based on the assumption (10) that $H \ll 1$. To calculate the salinity profile and the inner wall velocity for both this assumption and laminar flow, we would calculate the salinity at the inner wall from the temperature profile given by (17a) and (21a) and the Nernst condition. The inner wall velocity would then follow from (9). Because both our observations and our scale analysis show that the interior flow is convectively unstable, we shall not carry this laminar flow analysis beyond the present derivation.

7. Comparison of theory with experiment

We next compare the results derived in §§ 5 and 6 with our observations. First, in § 7.1, we show that the observed radius of the stalactite tip for a number of experiments agrees with the radius derived from (1). Second, to illustrate the convective instability of the flow inside the stalactite, in § 7.2 we discuss the inner wall temperature profiles for two stalactites, one with the temperature of

Experiment	Brine temperature and salinity	$\Delta\rho$ (g cm^{-3} $\times 10^{-2}$)	q (cm^3 s^{-1} $\times 10^{-1}$)	ν (cm^2 s^{-1} $\times 10^{-2}$)	a (cm $\times 10^{-1}$) Observed	a (cm $\times 10^{-1}$) Calculated	R_e
11 August	(20, 20)	15	1·66	4·5	1·0–1·2	1·1	21
3 March	(20, 20)	15	3·10	4·5	1·1–1·3	1·3	37
15 March	(20, 20)	15	5·2	4·5	1·5–1·6	1·5	49
16 March	(20, 20)	15	12·0	4·5	1·7–2·0	1·8	95
16 February	(5, 5)	3·5	3·0	2·0	1·9–2·1	1·5	48
17 February	(10, 10)	7	3·2	2·6	1·2–1·5	1·3	60
8 February	(15, 15)	1	3·13	3·3	1·4–1·6	1·2	40
9 February	(10, 15)	11	3·04	2·8	1·4–1·6	1·2	48
7 February	(10, 20)	15	3·04	3·6	1·2–1·3	1·2	45
3 February	(15, 20)	15	3·04	3·9	1·2–1·3	1·2	41

TABLE 3. Comparison of the observed and calculated values of the radius of the tip for the different experiments

the entering brine on the eutectic; the other with the temperature 10 °C above the eutectic. Our observations show as the flow becomes more unstable that the variation of wall temperature with depth increasingly deviates from a linear profile. Finally, in § 7.3, we compare the theoretical with the observed stalactite growth rates of both length and area, and show that, away from the stalactite entrance, the Graetz model gives a good approximation to the stalactite growth.

To simplify our description of the temperature and salinity of the entering brine, we shall give the brine salinity as the negative of its eutectic-point temperature, and the temperature as the positive depression below 0 °C. Thus, a (20, 20) brine has a salinity of 224‰ and a temperature of −20 °C.

7.1. *The entrainment number criterion*

As a test of the entrainment number criterion, we measured the inner radius of the tip for each of our stalactites, then compared the measured radius with the value calculated from (1). As we discussed in § 2, the tip size fluctuates during a given experiment. Therefore, for each particular run, we only measured the inner radius from those photographs on which the tip is a vertically oriented, circular pipe.

For all of the experiments, table 3 lists the density difference, the volume flux rate and the viscosity used to calculate E. $\Delta\rho$ is the difference between the density of the entering brine and the sea water, while the viscosity is the average of the entrance and sea-water values. As the table shows, our observations cover an order of magnitude in volume flux, and nearly the same range in density difference. For each of the runs, the sixth column lists the observed value of a; the seventh column, the value calculated from (1). The last column gives the Reynolds number of the flow in the tip.

With three exceptions, the calculated and measured values of the radii are in good agreement. The largest error occurs for the 16 February experiment. As figure 16 (plate 6) shows, this is a very slowly growing, short, stubby stalactite. Because of the short length, the interior flow is much less developed with higher

velocity shears at the wall than in the other stalactites. If we modelled these shears by increasing the value of ν in E, we would obtain a larger value of a. The other deviations occur for the 8 and 9 February experiments, both of which used salt solutions which freeze at $-15\,^{\circ}\mathrm{C}$. We have no explanation for this apparently real deviation of the predicted value from the measured one.

Because of both viscous effects and the instability of the interior flow, the flow inside the tip is not Poiseuille flow. Therefore, the agreement between the observed and predicted values of the radius from (1) with $E = 1$ is probably fortuitous, even though the functional form of E is very likely correct.

7.2. *Convection inside the stalactite*

To confirm the hypothesis that the flow inside the stalactite is unstable, we calculated both the inner wall temperature and the entrainment numbers for two experiments run with $q = 0{\cdot}3\,\mathrm{cm^3\,s^{-1}}$. For the first, 3 March, the entering brine is on the eutectic (20, 20); for the second, 7 February, the brine is $10\,^{\circ}\mathrm{C}$ above the eutectic (10, 20). Figures 5 and 6 (plates 1 and 2) show respectively the sequences of photographs of the stalactite growth for 3 March and 7 February.

Calculation of the temperature difference across the wall proceeds from (8) and the measured values of r_1 and r_2. On the photographs, we measured the values of r_1 and r_2 at depth intervals of 2 cm and time intervals of 60 s. Since our observations show that the stalactite is nearly always axially symmetric, we define $2r_1$ as the distance between the inner walls and $2r_2$ as the distance between the outer walls. The experimental accuracy of r_2 is $\pm 0{\cdot}02$ cm. Because we measure the inner radius through an ice wall, its accuracy is both less than that of the outer radius and decreases with increasing wall thickness. In general, the experimental accuracy of r_1 is less than or equal to $\pm 0{\cdot}05$ cm.

From these measurements, we then calculate the velocity from the 'centred difference' form of $\partial r_2/\partial t$. To choose L/k_i from table 2 for the two experiments, we assume for the 3 March experiment a mean wall temperature of $-8\,^{\circ}\mathrm{C}$, and for 7 February, a mean wall temperature of $-4\,^{\circ}\mathrm{C}$, where these values are consistent with our observed temperature profiles. From our data, these temperatures and table 2, we calculate T.

Figures 7 and 8 show the resultant temperature profiles. The width of the bars shows the uncertainty in the temperature caused by the measurement error of r_1 and r_2. In figure 7, the temperature difference with a few exceptions decreases along the stalactite length. In figure 8, the temperature profile has a very different appearance, being nearly constant away from both the tip and the beginning of the experiment.

To explain this difference between the two profiles, we calculate E for a few of the points on figures 7 and 8 in the following way. Given an outer wall temperature of $-2\,^{\circ}\mathrm{C}$, T_w follows from ΔT. From the Nernst condition, we then calculate the salinity, the density and the viscosity at the stalactite inner wall. Then, from (1), we calculate E based on the radius of the inner wall and the density difference between the inflowing brine and the fluid at the inner wall.

For the 3 March experiment, E ranges from 2 to 25 at all depths, with the smaller

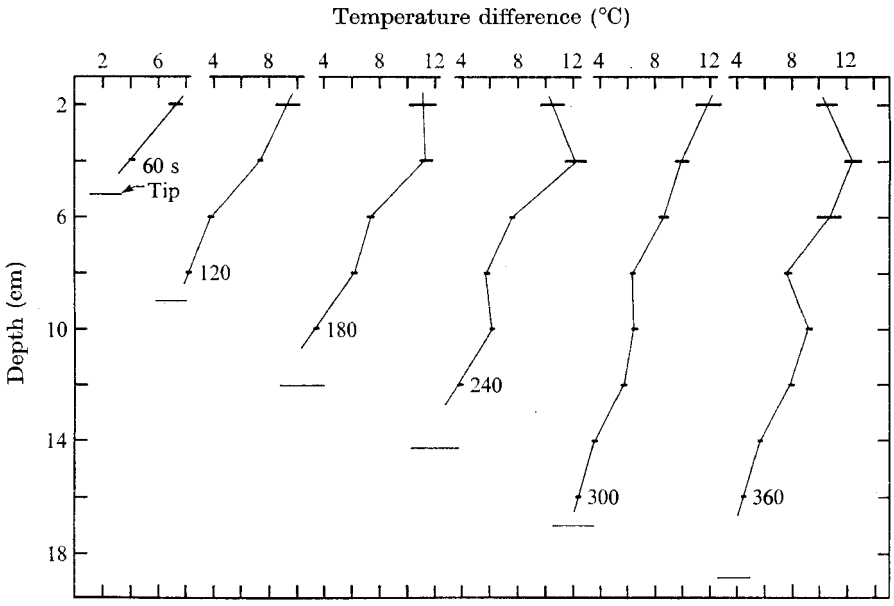

FIGURE 7. The temperature difference across the wall plotted versus time and depth from the 3 March stalactite. The horizontal lines below each temperature profile show the depth of the tip.

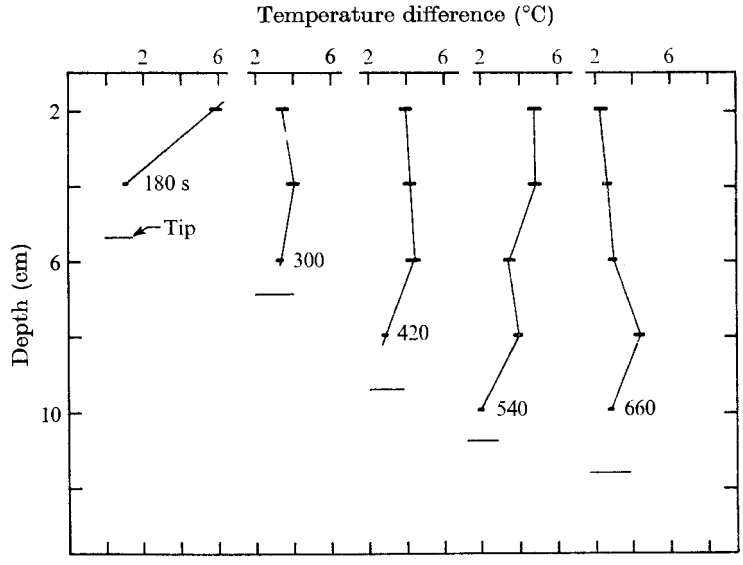

FIGURE 8. The temperature difference across the wall plotted versus time and depth for the 7 February stalactite.

values occurring at the tip, where r_1 is small, and at the entrance, where $\Delta\rho_w$ is small. Over most of the stalactite length, $E \sim 10$.

The 7 February experiment is much more convectively unstable. At a depth of 2 cm, for the times shown in figure 9, E ranges from 20 to 800, while at 10 cm, E ranges from 4 to 15. Over most of the length of the stalactite, $E \sim 10^2$. This

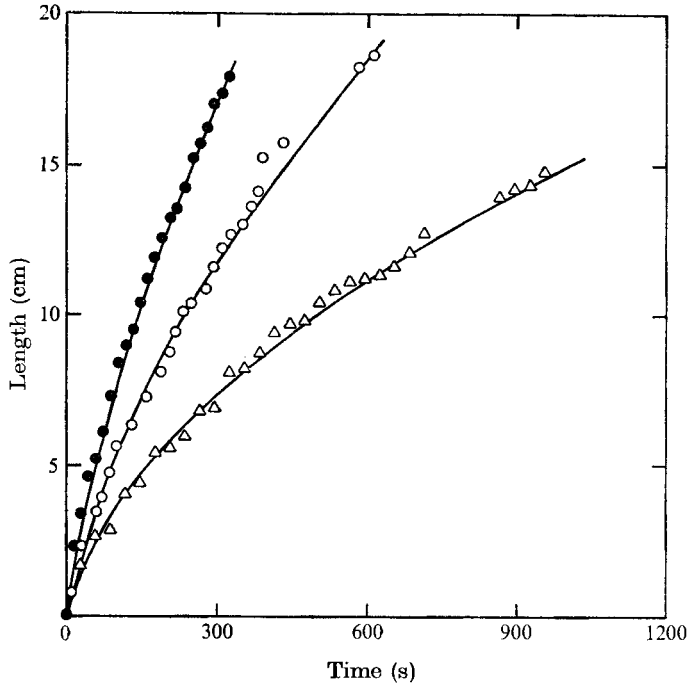

FIGURE 9. Comparison of the measured stalactite lengths with the theoretical growth curves for three runs with the same salinity and volume flux. Measured lengths: ●, 3 March; ○, 3 February; △, 7 February. ——, theory. The gaps in the measured points for 3 and 7 February occurred when we changed the film in the camera.

implies that the interior flow for 7 February is much more unstable than that of 3 March and explains the great difference in appearance between the two temperature profiles.

Examination of the stalactite photographs in figures 5 and 6 also shows evidence of convection. As seen in figure 6, the walls of the 7 February stalactite become slightly corrugated with time. From direct observation we associate the small bulges shown in the photographs with eddies caused by the rising, less dense fluid. The walls of the 3 March stalactite shown in figure 5 also display bulges, which are much less pronounced than those in figure 6. In summary, the temperature profiles, the values of E and the stalactite photographs suggest for both cases that the interior flow is unstable.

7.3. *Comparison of the observed and predicted growth rates*

Before we discuss the growth of the individual stalactites, we shall describe how we analysed our length observations. On the photographs, we defined the stalactite length as the distance from the base of the stalactite to the bottom of the longest crystal extending from the tip. To make this measurement was much easier than to try to determine for each photograph the depth at which the stalactite ceases to be a tube. We also neglect any curvature in the stalactite, but simply measure the length as a straight line from base to tip. The accuracy of this measurement is 2×10^{-2} cm.

Experiment	s (‰)	ΔT (°C)	q (cm^3 s^{-1} $\times 10^{-1}$)	l_0 (cm) Calculated	l_0 (cm) Observed	β (cm s$^{-\frac{1}{2}}$)	ζ (cm $\times 10^{-2}$)	$(l_0\zeta)^{-1}$ (cm^{-2})	α
7 February	224	7·5	3·04	16	2·6	0·55	4·3	8·8	0·55
3 February	224	13·0	3·04	16	7·0	1·00	2·7	5·3	0·70
3 March	224	17·6	3·10	16	9·1	1·40	2·5	4·4	0·95
15 March	210	16·4	5·25	28	4·7	1·20	2·9	7·4	0·52
11 August	226	18·0	1·66	8·8	4·0	0·92	2·2	11	0·65

TABLE 4. The parameters which describe the properties of the stalactites grown from brines with salinities approximately equal to 224 ‰

In most of our experiments, an equation of the form of (25*a*) with empirical values of l_0 and τ_0 describes the increase of the stalactite length. For each experimental run, we graphically fitted (25*a*) to our length measurements, and thus found empirical values of l_0, τ_0 and β. As (25*b*) shows, β describes the stalactite growth after a long time, whereas the values of l_0 and τ_0 determine the initial growth. Since a larger range of l_0 and τ_0 fits a particular initial growth than the range of β which fits the limiting growth, the accuracy of β is much greater than that of l_0 and τ_0. We found the experimental accuracy of β to be 3 %, whereas that of l_0 is 20 % and that of $\tau_0 = (l_0/\beta)^2$ is roughly 40 %. The other parameters of the stalactite growth, the areal slope ζ and the heat transfer coefficients ϵ and α, follow from our measurements of r_1 and r_2 versus length and time.

In the following discussion, we divide the experimental runs into three groups. First, we discuss those stalactites which we grew from brines with a constant salinity of 224 ‰, but with different values of ΔT and q. For $\Delta T \geqslant 8$ °C at this salinity, the stalactite walls were smooth enough so that measurements of r_1 and r_2 at 2 cm intervals in length gave representative values of the side-wall area.

Second, we discuss those stalactites for which we held the brine temperature constant and varied the salinity. These experiments divide into two runs at -15 °C, (15, 20) and (15, 15), and three runs at -10 °C, (10, 20), (10, 15) and (10, 10). The two stalactites grown at -15 °C were nearly identical, while the ones grown at -10 °C showed increasing departures from the Graetz theory as we approached the eutectic curve.

Finally, we discuss those stalactites grown from brines at -5 °C. Because none of these stalactites grew to a length greater than 5·5 cm, we only qualitatively discuss these observations.

7.3.1. *The experiments run at* 224 ‰. As table 4 shows, these experiments consist of three runs at a constant flow rate, but different brine temperatures, and two additional runs at the same temperature, but different flow rates. In the following discussion, we shall first discuss the growth in length and then discuss the growth in side-wall area for these experiments.

For the first three runs, figure 9 compares the measured stalactite lengths with the empirically fitted growth curves. Examination of the figure shows that

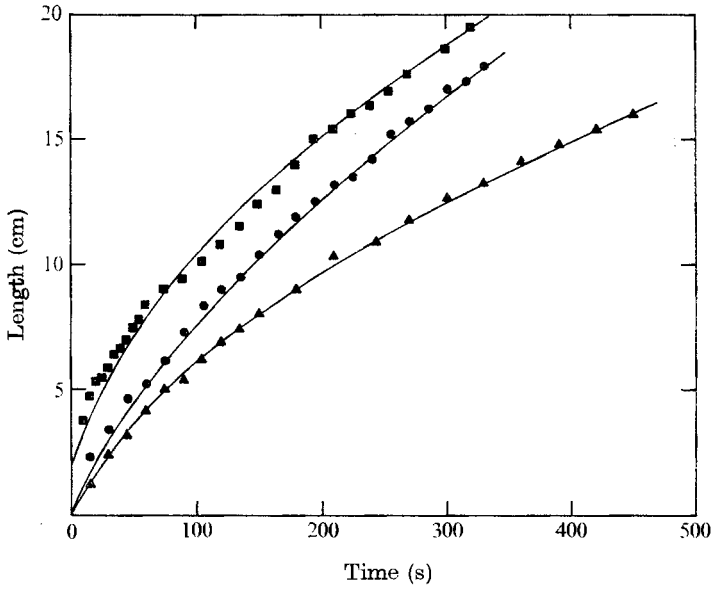

FIGURE 10. Comparison of the measured stalactite lengths with the theoretical growth curves for three runs with the same salinity and temperature, but different volume fluxes. Measured lengths: ■, 15 March; ●, 3 March; ▲, 11 August. ——, theory. For clarity, the length origin of 15 March is offset 2 cm vertically above the origin.

the curves and the experimental points are in good agreement. Table 4 lists the values of l_0 and β used in the calculation of the empirical curves, and compares the theoretical and measured values of l_0. As the temperature of the inflowing brine approaches the freezing point, the experimental value of l_0 increases to roughly one half of its calculated value. The decrease in l_0 with temperature difference suggests from (19) and (20) that the Nusselt number increases as we lower the temperature of the entering brine below the eutectic curve.

Flow rate changes have a more complicated effect on the growth than temperature changes. For the last three experiments in table 4, which are run at nearly the same temperature, figure 10 compares the measured growth rates with the empirical curves, and figure 11 (plate 3) shows sequential photographs of the 15 March stalactite. Examination of table 4 shows that the ratio of the observed to the theoretical value of l_0 is nearly the same for the 3 March and 11 August experiments, while much less for the higher flow rate of 15 March. Both figure 10 and the values of β listed in table 4 show that 15 March stalactite grew at a slightly slower rate than that of 3 March.

Increased mixing generated by the larger volume flux of 15 March over that of 3 March probably causes the slower growth rate of 15 March. If we calculate the entrainment number E based on the inlet tube radius for the initial flow of brine into the tank, we find $E = 1{\cdot}2$ for 3 March and $E = 0{\cdot}72$ for 15 March. Therefore, the initial flow from the inlet tube for 15 March is unidirectional, with a Reynolds number which we calculate as $R_e = 33$. Rouse (1961, p. 259) shows that the flow of a constant-density fluid through an abrupt change of cross-section with $R_e \gtrsim 10^2$ generates an axisymmetric vortex. In figure 11, this vortex probably

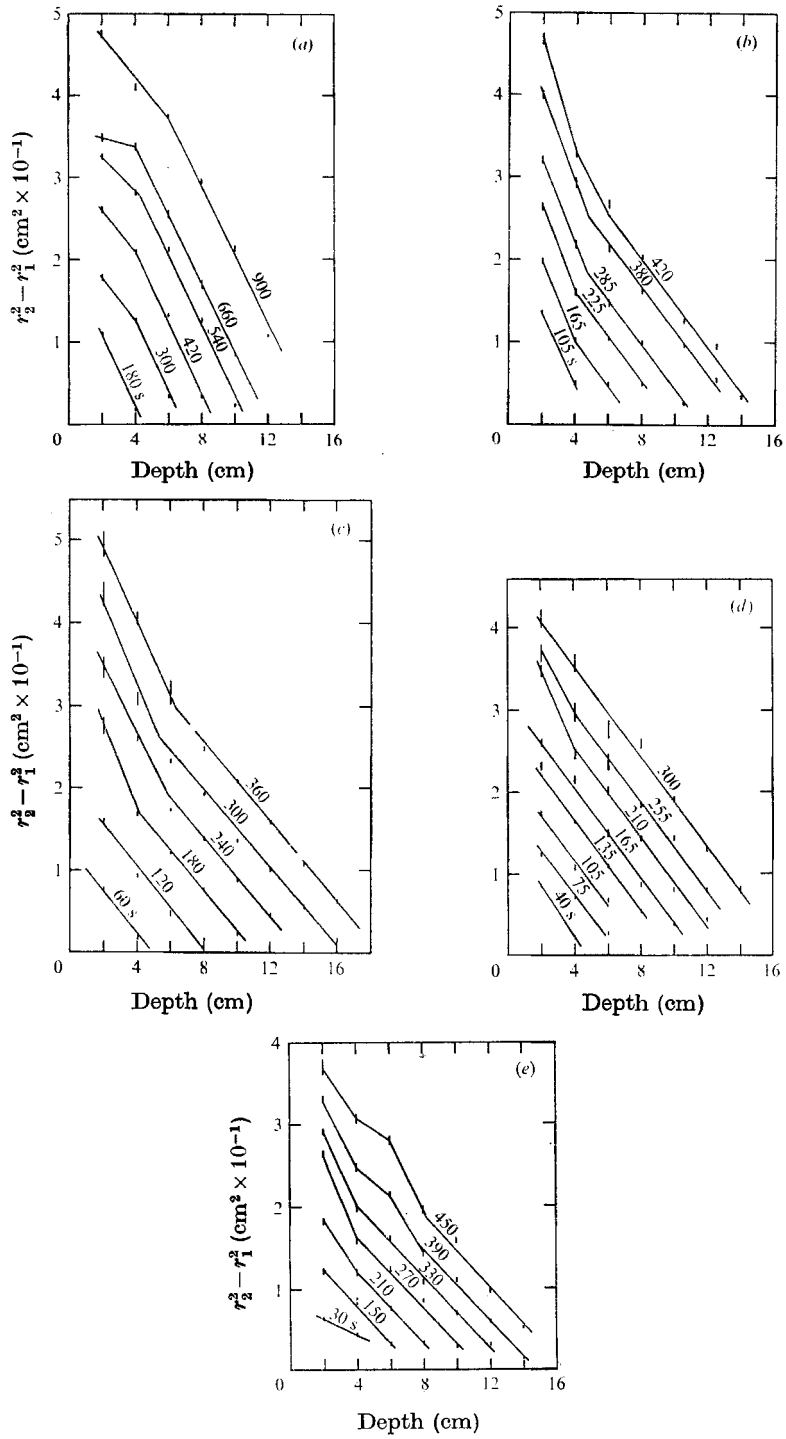

FIGURE 12. The side-wall area plotted versus time and depth. The vertical bars are the measured points, where the height of the bar indicates the measurement uncertainty; the thin continuous lines connect points measured at the same time. (*a*) 7 February, (*b*) 3 February, (*c*) 3 March, (*d*) 15 March, (*e*) 11 August.

is the cause of both the pronounced bulge near the entrance which is absent from the 3 March stalactite and the smaller values of l_0 and β for 15 March.

For the same five experiments, we next discuss the growth in side-wall area. Figures 12(*a*)–(*e*) display the side-wall areas plotted versus length and time. On the figures, the vertical bars are the data points, while the continuous lines connect points measured at the same time. Away from both the entrance and the very beginning of the experiment, the figures show that straight lines drawn parallel to one another fit the experimental points, so that the areal slope is constant. This constancy, combined with our observation that the length growth rate has the same form as (24), means from (26)–(31) that the averaged side-wall heat flux is independent of position.

The deviations from constant slope generally occur near the stalactite entrance. For the three experiments, 3 February, 3 March and 11 August, shown respectively in figures 12(*b*), (*c*) and (*e*), more ice forms with time near the entrance than further down the stalactite. Because the brine enters the stalactite with a constant temperature, rather than the Graetz temperature profile of (17*b*), both the temperature gradients and thereby the ice growth are much larger near the entrance than further down the stalactite.

For the 7 February case, or figure 12(*a*), less ice forms near the top of the stalactite than further down. Of the five cases shown, that of 7 February is the most convectively unstable. We therefore expect that the warm, less saline brine which forms at the inner wall flows up the wall and collects at the top of the stalactite. Here the warm brine serves as a buffer between the incoming cold brine and the ice walls, so that freezing may take place in the interior and the walls move outward with less accretion than further down the stalactite.

The last three columns in table 4 list the parameters related to the amount of ice rejected by the stalactite. Specifically, the eighth column gives the value of ζ measured from a graphical fit of straight lines to the data shown in figure 12. The accuracy of ζ is $\pm 0{\cdot}1 \times 10^{-2}$ cm, so that, for example, the measured slopes for 3 March and 3 February are equal to within the experimental error. Because these two runs are identical except for a 5 °C difference in entrance temperature, this agreement of the slopes is to be expected.

Given ζ, we next calculate the coefficients α and ϵ. From (31),

$$\epsilon = (b^2 - a^2)/l_0\zeta.$$

At the stalactite tip, because the photographic image of the crystals which make up the tip tends to fade into the grain size of our negatives, we could only estimate the parameter $b^2 - a^2$. From the photographs $b - a \sim 10^{-2}$ cm, and since in most of our experiments $a \sim 10^{-1}$ cm, we estimate $b^2 - a^2 \sim 10^{-3}$ cm^2. The next-to-last column of table 4 lists the values of $(l_0\zeta)^{-1}$ for the various runs. Since $b^2 - a^2 \sim 10^{-3}$ cm^2 and $(l_0\zeta)^{-1} \sim 10$ cm^{-2}, we find that

$$\epsilon \sim 10^{-2}.$$

As a first approximation, then, all of the ice represented by the mixed-mean temperature deficit at the tip goes into the ocean.

Second, we discuss the coefficient α, which measures the amount of ice

Experiment	s (‰)	ΔT (°C)	q (cm^3 s^{-1} $\times 10^{-1}$)	l_0 (cm) Calculated	l_0 (cm) Observed	τ_0 (s) Observed	β (cm s$^{-\frac{1}{2}}$)
3 February	224	13·0	3·04	16	7·0	49·0	1·00
8 February	188	12·5	3·13	16	7·0	54·0	0·96
7 February	224	7·5	3·04	16	2·6	23·0	0·55
9 February	188	7·8	3·04	16	1·3	9·0	0·43
17 February	140	7·8	3·17	16	0·3	0·4	0·43

TABLE 5. The parameters which describe the increase in length for stalactites grown from brines with nearly the same temperatures, but different salinities

rejected to the ocean by both freezing in the interior and the breaking-off of ice crystals at the tip. If we write ϵ in terms of l_0 and τ_0 from (20a, b), then substitution of ϵ from (31) gives

$$\alpha = \pi\beta^2\zeta/2qF, \tag{32}$$

where $\beta^2 = l_0^2/\tau_0$. To interpret α physically, we note for $t \gg \tau_0$ that

$$\alpha = \tfrac{1}{2}\pi\zeta l^2/qFt, \tag{33}$$

which is the ratio of the volume of ice grown by heat conduction to the maximum possible volume of ice, so that $\alpha < 1$.

As the last column of table 4 shows, with the exception of the 3 March case, the values of α range from 0·5 to 0·7. The larger value of α derived for 3 March may be caused by a slight supercooling of the sea water; we observed an unusually heavy ice cloud for this experiment.

For the 11 August stalactite, we also compute from a direct recovery at 480 s the fraction of ice which went into stalactite growth. At 480 s, the maximum possible ice volume V_m is $V_m = qFt = 21{\cdot}6\,\text{cm}^3$. Since we observed an ice volume of 13·6 cm^3, the 11 August stalactite at 480 s consisted of only 0·63 of the available ice. In summary, the calculated values of α and ϵ, the direct measurement of the stalactite volume and our observations of the ice crystals being swept downstream from the stalactite tip show that a large fraction of the potential stalactite ice goes into the ocean.

7.3.2. *The experiments run with T and q constant.* In the previous subsection, we described the changes in the stalactite growth when, for a fixed salinity, we decreased the temperature difference below the eutectic curve. In this subsection, we next describe what happens when, for two fixed temperatures, we decrease the salinity difference in 5 °C steps until we reach the eutectic.

Table 5 lists the properties of the experiments, two of which, those on 3 and 7 February, we discussed in the previous section. The first two experiments in table 5 were run at (15, 20) and (15, 15) respectively. Examination of the parameters shows that the stalactites grew at almost identical rates; in fact, when we superimposed the plots of length versus time, the points lay on top of one another. The stalactites were also very similar in appearance.

At -10 °C, the temperature at which we ran the next three experiments in table 5, the stalactite appearance changed greatly as we decreased the salinity

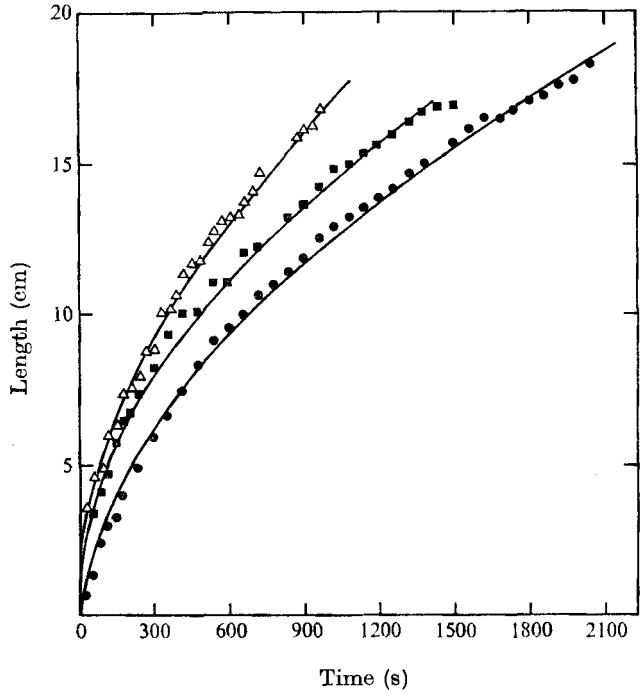

FIGURE 15. Comparison of the measured stalactite lengths with the theoretical growth curves for three experiments run at -10 °C, $q = 3 \times 10^{-1}$ cm^3 s^{-1}, but different salinities. Measured lengths: △, 7 February; ■, 9 February; ●, 17 February. For clarity, the length origins for 7 and 9 February are offset respectively 2 and 1 cm above the indicated origin.

toward the eutectic. For these experiments, the last three lines in table 5 show the growth parameters, figures 13 and 14 (plates 4 and 5) respectively show the stalactite sequences for 9 Feburary and 17 February, and figure 15 compares the measured lengths with the fitted curves. As both table 5 and figure 15 show, even though the 7 February experiment was run at a slightly lower volume flux and temperature difference than the other two experiments, the length of the stalactite grew slightly faster. Also, the value of l_0 decreased as we lowered the salinity for these three experiments. To explain the difference between these experiments, we examine the growth of the side walls. Because the walls in the photographs of 9 February and 17 February were too corrugated to permit a representative sampling of the side-wall area at length intervals of 2 cm, we compare these stalactite photographs only qualitatively.

The major difference between the 9 and 17 February stalactite is that a large bulge develops with time at the top of the former while the wall thickness of the bulge becomes very thin. At a depth of 0·9 cm from the stalactite base, which is slightly above the centre of the bulge at 36 min, we calculated ΔT at both 4·5 and 36 min. At 4·5 min, $\Delta T = 6$ °C, while at 36 min, $\Delta T = 1$ °C, so that, as the experiment progressed, the bulge filled with relatively warm water.

The cold brine enters the stalactite from the inlet pipe with a radius of 1·5 mm along the centre-line of the stalactite. The temperature measurement suggests

that the warmer, less saline water formed at the inner wall rises to the top. Here the combination of the abrupt expansion section between the inlet tube and the stalactite base, the cold brine descending at the centre and the warmer brine rising at the inner wall causes the formation of an axisymmetric eddy. Because the temperature of the entering brine is above the eutectic curve, and if the mixing causes salinity and temperature to be transferred at nearly the same rates, then the warmer, less saline water can transfer heat to the inflowing brine without necessarily causing freezing. If freezing does occur, the crystals may form in the stalactite interior, then be swept out of the stalactite.

The 17 February stalactite in figure 14 has a very different appearance. Just below the entrance, there is a small bulge, but below this bulge, as shown in both the front and side view at 30 min, an ice plug forms. For this case, the warmer, less saline brine generated by the outward motion of the wall again rises up the stalactite. Because both the rising and the inflowing brines are very near their respective freezing points, freezing occurs when heat is transferred between them, thus generating the ice plug. Obviously, our simple Poiseuille flow model describes neither the bulge in figure 13, nor the ice plug in figure 14.

7.3.3. *The experiments run at* $T = -5\,^{\circ}\mathrm{C}$ *and* $q = 3 \times 10^{-1}\,\mathrm{cm^3\,s^{-1}}$. At this temperature and volume flux, we ran four experiments using brine salinities of 224, 188, 140 and 79‰. With the exception of the 79‰ case, we found it almost impossible to grow stalactites at this temperature.

For $s = 224$‰, we could only grow a stalactite by first growing from a colder brine a stalactite of about 1 cm in length, into which we then pumped the $-5\,^{\circ}\mathrm{C}$ brine. The original stalactite began to grow in radius, but not in length. As the inner radius increased and the interior flow became more convectively unstable, sea water intruded into the stalactite, until suddenly there was a turbulent overturning which flushed most of the dyed water from the stalactite. At this point, the cold brine flowed down one side of the original stalactite and grew a second ice tube around itself, which again grew slowly in length and inner radius. When the new stalactite reached a length of about 1 cm, turbulent overturning again occurred, and the process began again. The entire cycle, from overturning to overturning, took roughly 30 min.

At $s = 188$ and 140‰, neither stalactite grew more than a few millimetres; we observed when crystals protruded beyond the circular base that shear stresses broke them off.

Finally, figure 16 (plate 6) shows the 16 February stalactite, where $s = 79$‰; this was the only stalactite in this series to grow more than 1 cm in length. This stalactite grew very slowly in time. At 42 min, as shown on the photograph by both the reflecting intrusion of sea water at the tip and the freezing of sea water at the stalactite entrance, overturning occurred. From this point on, the stalactite stopped growing in length as the sea water in the interior froze around the cold brine.

In summary, this series of experiments suggests that because of the development of extremely unstable interior flows, stalactites grown from brines with small temperature differences do not grow beyond some small length.

8. Concluding remarks

In summary, the combination of the Graetz stalactite solution with the entrainment number criterion for both the radius of the tip and the onset of convection inside the stalactite gives a good description of how stalactites grow from brines colder than $-15\,^{\circ}\mathrm{C}$. At brine temperatures of order $-10\,^{\circ}\mathrm{C}$, the results of the previous section show that convective instabilities become important, and although the Graetz solution still describes the stalactite length, the side-wall areal slope is no longer constant. Finally at $-5\,^{\circ}\mathrm{C}$, the convective instabilities overwhelm the Graetz solution, and our observations suggest that the stalactite grows only a short distance in length.

These results have a number of implications for studies of the polar pack ice. First, the entrainment number criterion shows that field measurements of the volume flux out of a stalactite can be made from a photograph of the tip to determine the inner radius and a water sample to determine ν and $\Delta\rho$. Second, the results of the previous section suggest that the brine must be colder than $-5\,^{\circ}\mathrm{C}$ for stalactites to grow to a length greater than 10 cm. The observations of much longer stalactites in the polar oceans therefore suggest that brines with salinities of the order of 100‰ drain from the ice. In McMurdo Sound, Paige (1970) estimated the stalactite density as "three or four in an area of about $25\,\mathrm{m}^2$". Whether the occurrence of dense brine plumes with this spatial frequency could contribute in any significant way to the formation of the Antarctic bottom water is an open question.

Third, the loose ice crystals rejected by the ice stalactites, which our experiments show may equal as much as one half of the total amount of ice represented by the cold brine, may affect the properties of natural sea ice. In a survey paper, Lewis & Weeks (1971) point out that the Antarctic ice cover, unlike the Arctic, consists in some locations of ordinary sea ice over a layer of loosely packed ice crystals. They cite one observation near Mirny where this crystal layer had a thickness of 4 m under 1 m of sea ice. The present accepted explanation of this crystal layer is that the cold ice shelves generate the crystals; another possibility comes from the interaction of the loose stalactite crystals with supercooled sea water. Lewis & Weeks also summarize, albeit sceptically, the numerous observations of supercooled water reported at depths down to 50 m in both polar oceans. Given these observations, the ice crystals which accompany the stalactite growth and are swept into the interior by the brine plumes could serve as nucleation sites for the supercooled water. The much larger crystals would then float to the bottom of the pack ice to form the crystal layer.

I thank Lawrence Larsen and Creighton A. Depew for discussions about the theory. The experiments were done with the assistance of Donald Immerwahr; I greatly appreciate both his persistence and ingenuity in designing the photographic techniques described in § 3. For their general help and support, I thank Beverly Garrick, Meriam Lorette and Norbert Untersteiner. Finally, I gratefully acknowledge the support of the Arctic Program of the Office of Naval Research under Project NR307-252 and Contract N00014-67-A-0103-0007, Con-

tribution 740 of the Department of Oceanography, University of Washington, and Contribution 296 of the Department of Atmospheric Sciences, University of Washington.

REFERENCES

BAKER, D. J. 1966 A technique for the precise measurement of small fluid velocities. *J. Fluid Mech.* **26**, 573.

CARSLAW, H. S. & JAEGER, J. C. 1959 *Conduction of Heat in Solids.* Oxford University Press.

DAYTON, P. K. & MARTIN, S. 1971 Observations of ice stalactites in McMurdo Sound, Antarctica. *J. Geophys. Res.* **76**, 1595.

EIDE, L. I. & MARTIN, S. 1974 The formation of brine drainage features in young sea ice. Submitted to *J. Glaciol.*

ELLISON, T. H. & TURNER, J. S. 1959 Turbulent entrainment in stratified flows. *J. Fluid Mech.* **6**, 423.

FRANK, F. C. 1950 Radially symmetric phase growth controlled by diffusion. *Proc. Roy. Soc.* A **201**, 586.

GOLDSTEIN, S. 1938 *Modern Developments in Fluid Mechanics*, vol. 2. Dover.

HALLMAN, T. M. 1958 Combined free and forced convection in a vertical tube. Ph.D. thesis, Purdue University (University Microfilms, L.C. Card no. Mic 58-3160, Ann Arbor, Michigan).

KAUFMAN, D. W. 1960 *Sodium Chloride.* Reinhold.

KAYS, W. M. 1966 *Convective Heat and Mass Transport.* McGraw-Hill.

LAKE, R. A. & LEWIS, E. L. 1970 Salt rejection by sea ice during growth. *J. Geophys. Res.* **75**, 583.

LEWIS, E. L. & WEEKS, W. F. 1971 Sea ice: some polar contrasts. In *Symp. on Antarctic Ice & Water Masses* (ed. G. Deacon), pp. 28–38. Scott Polar Research Institute, University of Cambridge.

ONO, N. 1967 Specific heat and heat of fusion of sea ice. In *Physics of Snow and Ice*, vol. 1 (ed. H. Oura), pp. 589–610. Institute of Low Temperature Science, Hokkaido University, Japan.

PAIGE, R. A. 1970 Stalactite growth beneath sea ice. *Science*, **167**, 171.

ROUSE, H. 1961 *Fluid Mechanics for Hydraulic Engineers.* Dover.

SCHEELE, G. F. & HANRATTY, T. J. 1963 Effect of natural convection instabilities on rates of heat transfer at low Reynolds number. *A.I.Ch.E. J.* **9**, 183.

SCHEELE, G. F., ROSEN, E. M. & HANRATTY, T. J. 1960 Effect of natural convection on transition to turbulence in vertical pipes. *Can. J. Chem. Eng.* **38**, 67.

SCHLICHTING, H. 1962 *Boundary Layer Theory.* McGraw-Hill.

SCHWERDTFEGER, P. 1963 The thermal properties of sea ice. *J. Glaciol.* **4**, 789.

WEEKS, W. F. 1968 Understanding the variations of the physical properties of sea ice. In *Symp. on Antarctic Oceanography* (ed. R. Currie), pp. 173–191. Scott Polar Research Institute, University of Cambridge.

WEEKS, W. F. & LOFGREN, G. 1967 The effective solute distribution coefficient during the freezing of NaCl solutions. In *Physics of Snow and Ice*, vol. 1 (ed. H. Oura), pp. 579–599. Institute of Low Temperature Science, Hokkaido University, Japan.

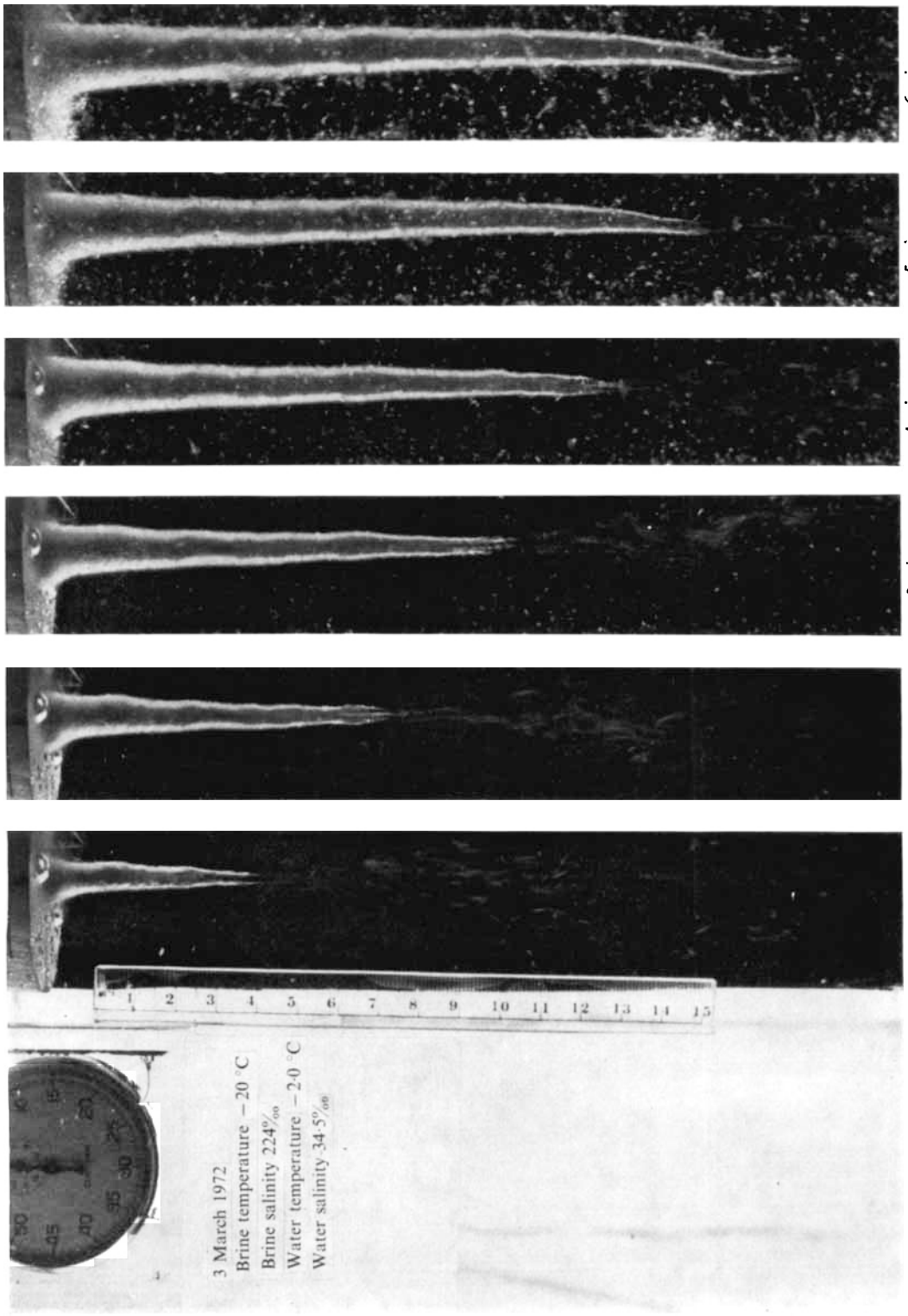

FIGURE 5. A sequence of stalactite photographs taken on 3 March 1972: $s = 224$ ‰, $T = -20$ °C, $q = 3{\cdot}1 \times 10^{-1}$ cm^3 s^{-1}. The small white particles are free ice crystals generated by the cold brine which are swept to the bottom of the tank and then rise to the surface.

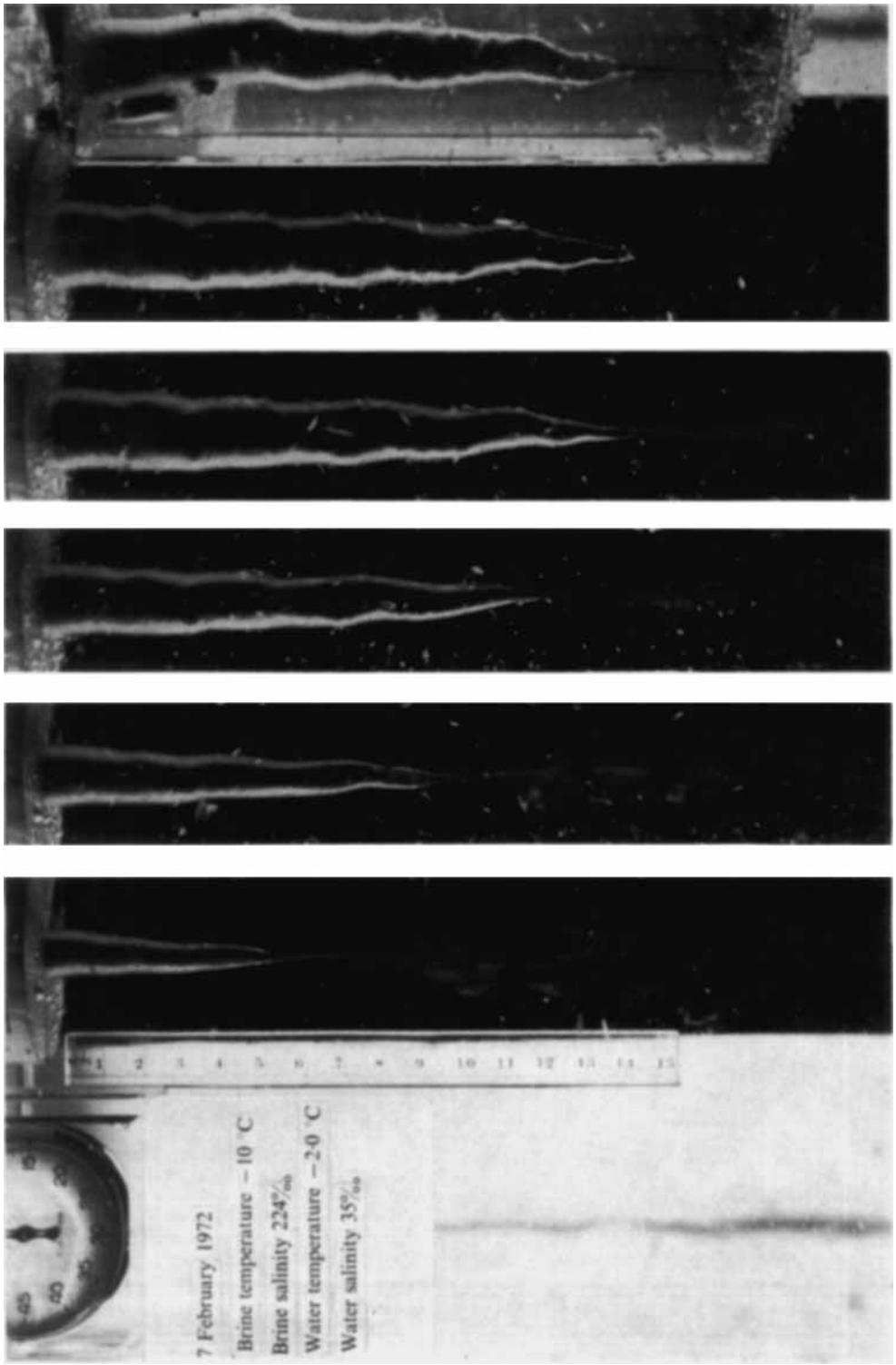

FIGURE 6. The sequence of stalactite photographs taken on 7 February 1972: $s = 224\,‰$, $T = -10\,°C$, $q = 3{\cdot}1 \times 10^{-1}\,cm^3\,s^{-1}$.

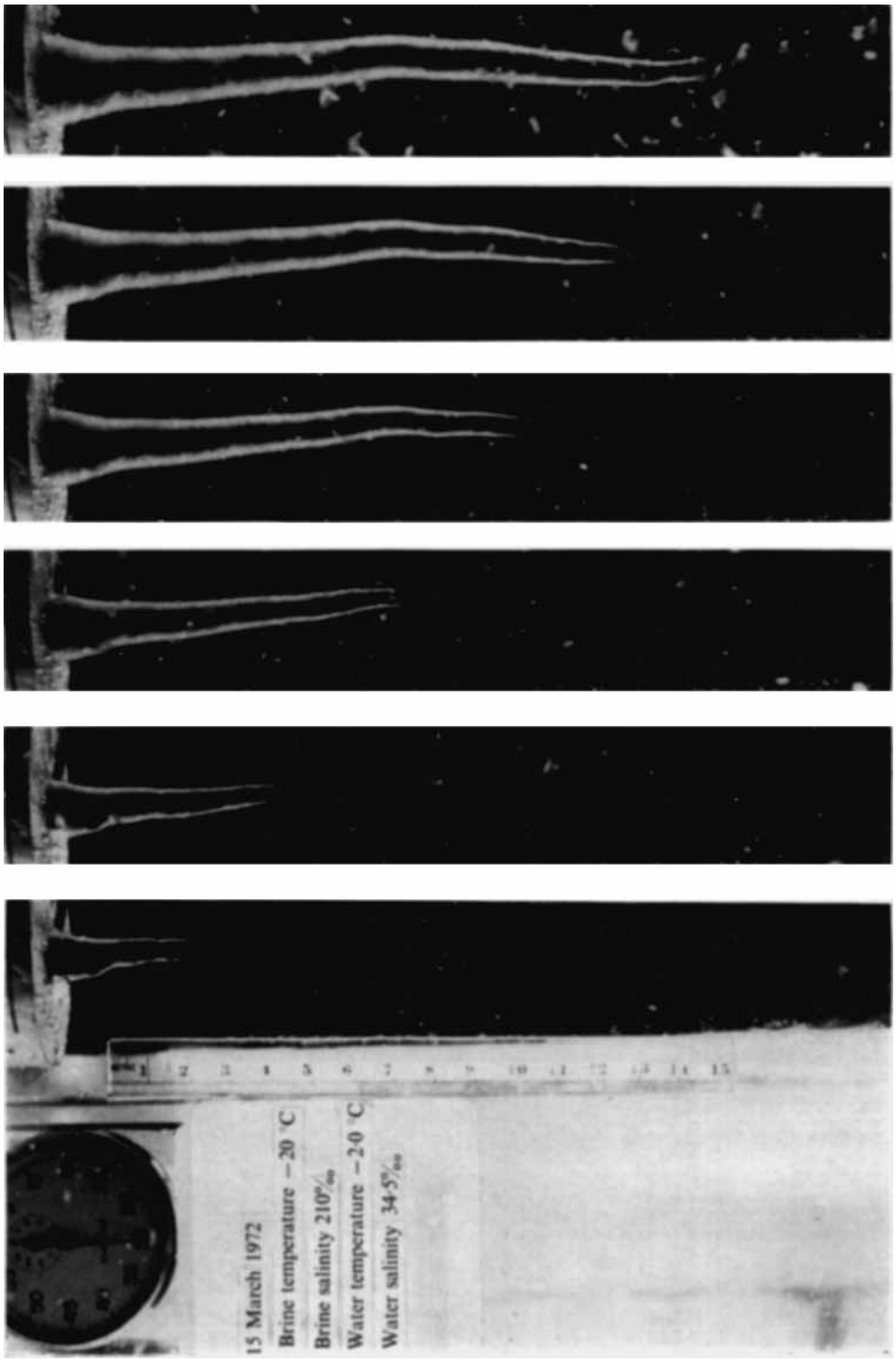

FIGURE 11. A sequence of stalactite photographs taken on 15 March 1972: $s = 210\,‰$, $T = -18{\cdot}4\ ^{\circ}\mathrm{C}$, $q = 5{\cdot}25 \times 10^{-1}\ \mathrm{cm^3\ s^{-1}}$.

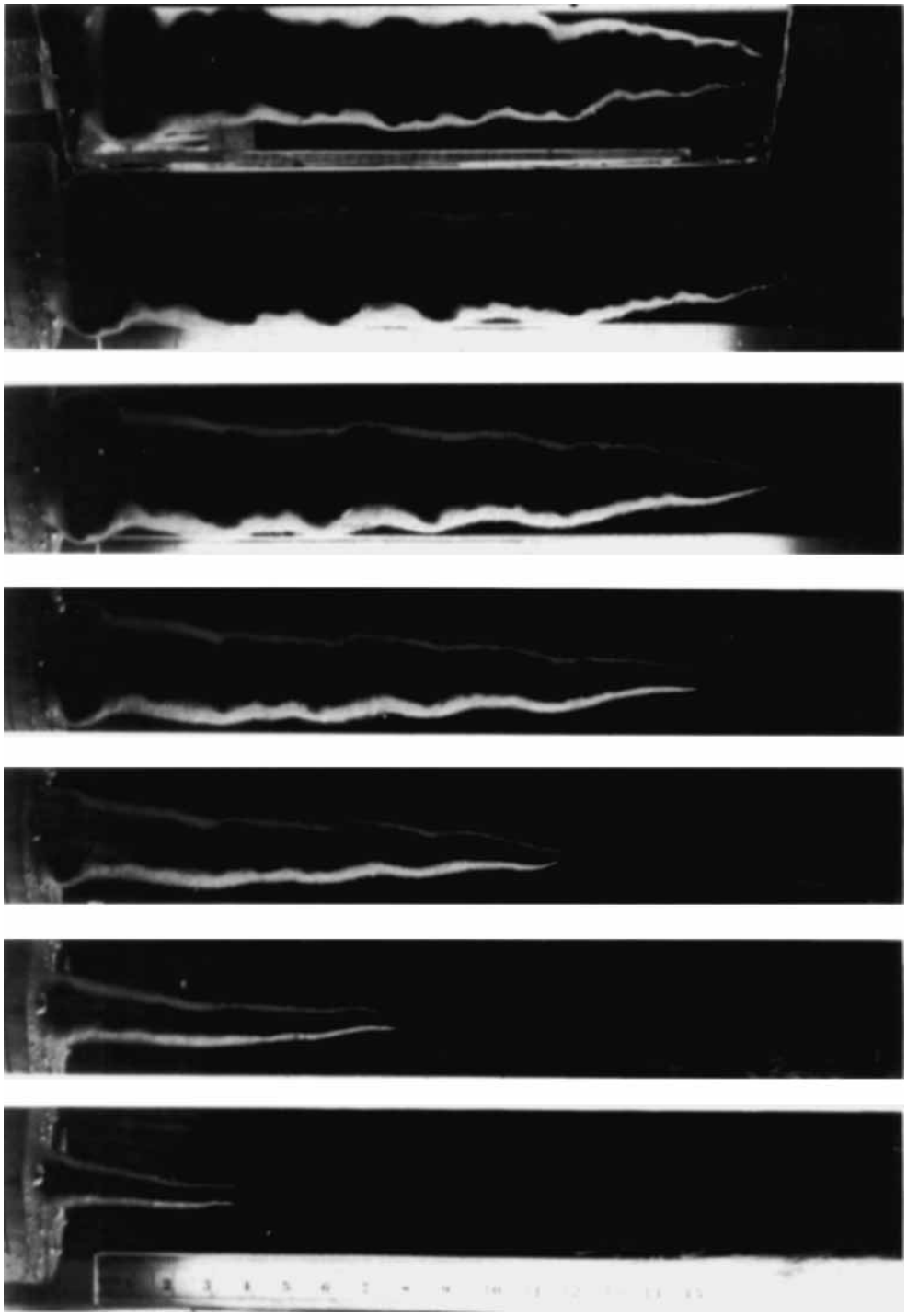

FIGURE 13. A sequence of stalactite photographs taken on 9 February 1972: $s = 188\,‰$, $T = -9{\cdot}8$ °C, $q = 3{\cdot}04 \times 10^{-1}$ cm^3 s^{-1}. The photograph taken at 47 min shows both the front and side view of the stalactite.

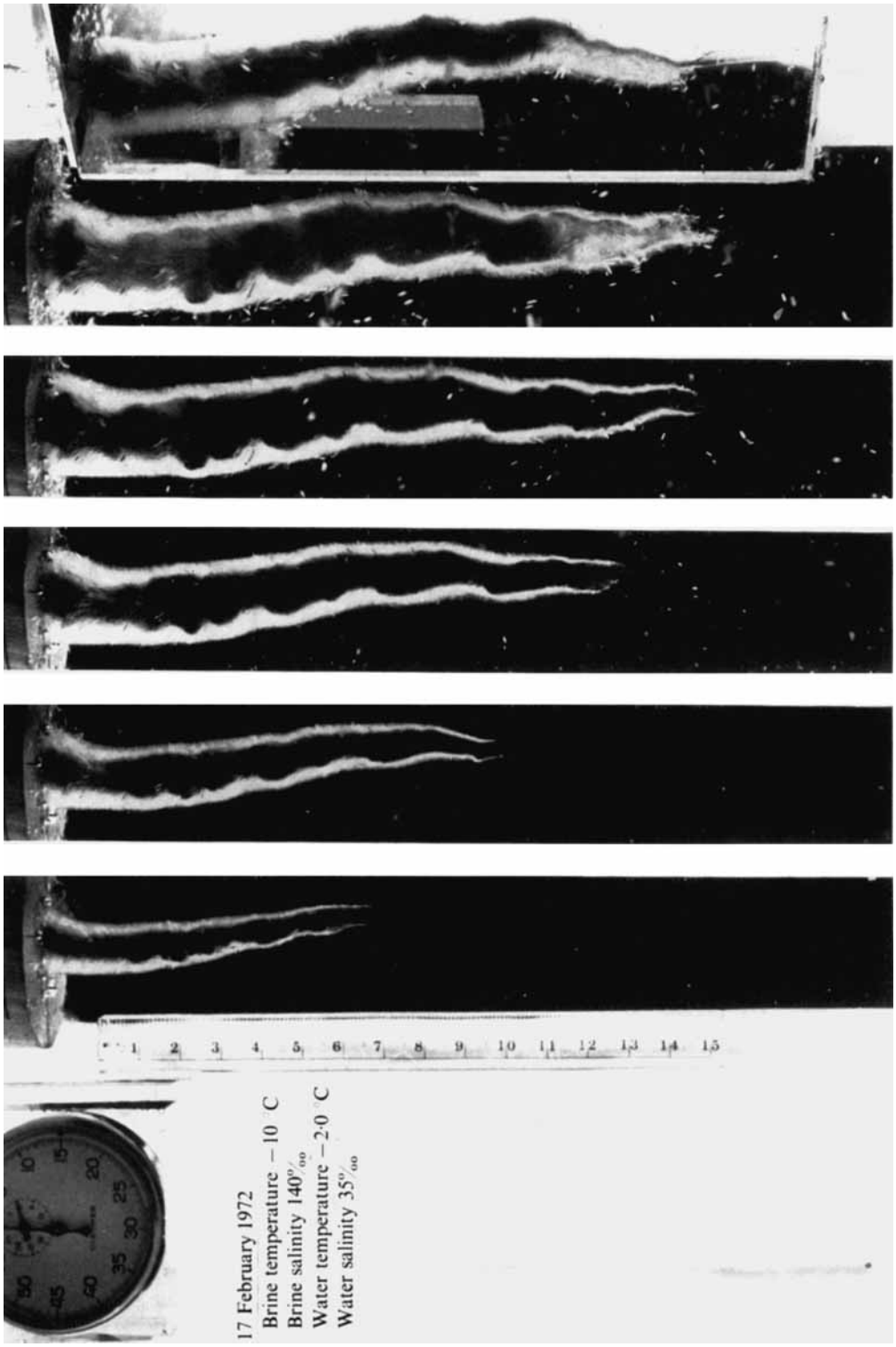

FIGURE 14. A sequence of stalactite photographs taken on 17 February 1972: $s = 140\,‰$, $T = -9{\cdot}8\,^{\circ}\mathrm{C}$, $q = 3{\cdot}2 \times 10^{-1}\,\mathrm{cm^3\,s^{-1}}$.

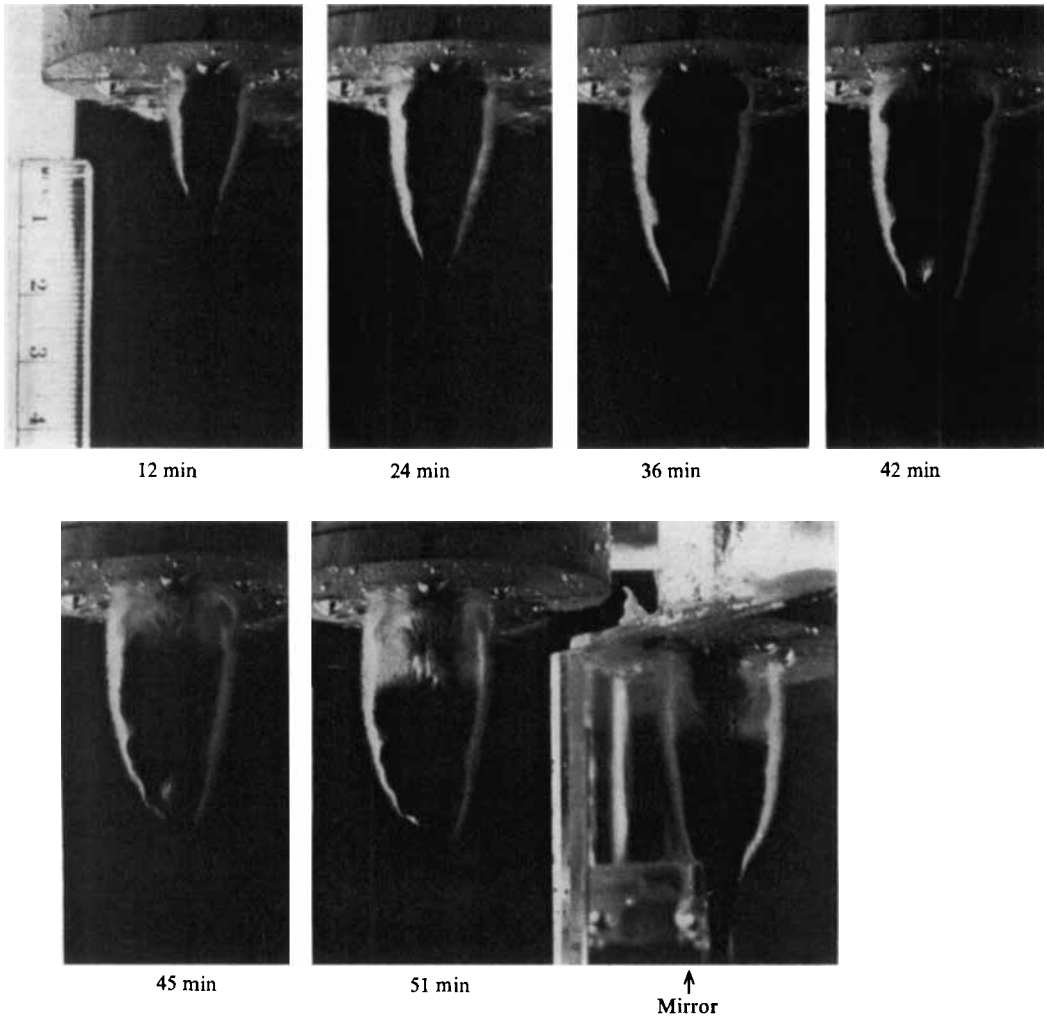

FIGURE 16. A sequence of stalactite photographs taken on 16 February 1972: $s = 79\,‰$, $T = -5\,^{\circ}\mathrm{C}$, $q = 3{\cdot}0 \times 10^{-1}\ \mathrm{cm^3\ s^{-1}}$.